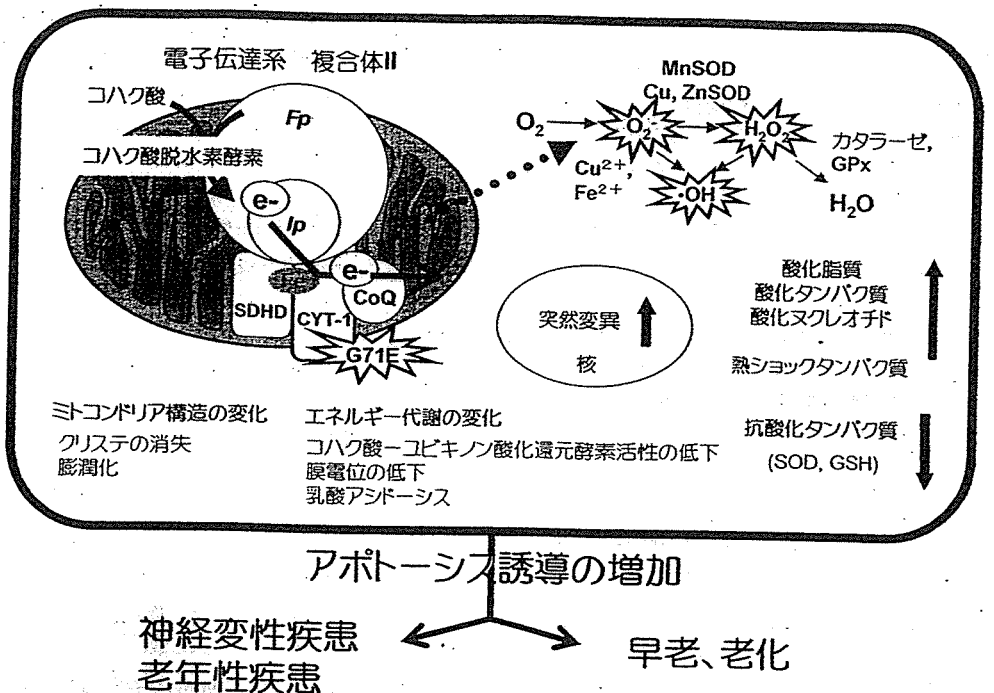

図2 *C. elegans*, *mev-1* 変異体の表現型

て有用となることが示された（図2）.

疾患モデル動物としての *C. elegans*, *mev-1* 変異体

C. elegans は雌雄同体が基本であり，染色体不分離によ 800匹に1匹の割合で雄が生まれる．雌雄同体の *C. egans* は孵化時に558個の体細胞からなり，幼虫期の間 一部の細胞が分裂して，最終的に個体差のない959個の められた細胞数からなる成虫になる．実際には受精卵か 成虫になるまでに1,090個の細胞が作られるが，そのう 131個の細胞が発生過程におけるプログラム細胞死によ て失われる．成虫では生殖幹細胞のみが細胞分裂を継続 る．したがって，*C. elegans* の体細胞はヒトなどの哺乳 における非分裂系細胞（神経細胞や筋肉細胞など）のモ ルになると考えられ，神経変性疾患のモデル動物として 用視されてきた．

ミトコンドリア病とはミトコンドリアの機能異常によ 発症する病態を総称して指す．その中でミトコンドリア に代表されるCPEO (chronic progressive external hthalmoplegia)，MELAS (mitochondrial encephalo-ropathy, lactic acidosis, and stroke-like episodes)，お びMERRF (myoclonus epilepsy associated with rag-l-red fibers) は電子伝達系酵素活性の欠損症に分類さ ている．これらは，主としてミトコンドリアDNA異常 より複合体IやIVに機能欠損が認められている[14]．一 染色体DNA由来のサブユニットで構成されている複 体IIの機能欠損によるミトコンドリア病には，Fpサブユニットの機能欠損によるLeigh脳症が報告されている[15]．また，神経変性疾患の発症にも電子伝達酵素活性の低下などによるミトコンドリア機能不全が関与することが報告されている．複合体II酵素活性に異常が認められる症例には，アルツハイマー病，パーキンソン病，ハンチントン病などが報告されている[16~18]．

このように，ミトコンドリア病をはじめ，さまざまな神経変性疾患の発症機序にミトコンドリア機能不全が関与しており，電子伝達系複合体II酵素活性の低下が確認されている *C. elegans* の *mev-1* 変異体は上記した疾患発症の機序解明のモデル動物になると期待されている．

4. マウス胎児細胞，SDHC E69変異細胞株

1) SDHC V69Eアミノ酸点変異を有した細胞株の樹立

C. elegans, *mev-1* 変異体の原因遺伝子産物であったCYT-1アミノ酸配列の相同検索を行い，マウスSDHCのアミノ酸配列（DDBJ database accession numbers AK032458-1 for *Mus musculus*）を取得し，コハク酸-ユビキノン酸化還元酵素活性領域，ユビキノンやヘム結合領域などの特性領域において約80%の相同性があることを確認した．*mev-1* 変異体においてアミノ酸点変異（G71E）が生じた部位は塩基性アミノ酸に富むユビキノン結合領域内に存在し，酸化還元酵素タンパク質の活性中心領域で求核性アミノ酸として働くセリン残基や，ユビキノンとの結合に必須のヒスチジン残基に隣接していた（図3）．したがって，これらに隣接した部位に存在する中性アミノ酸を

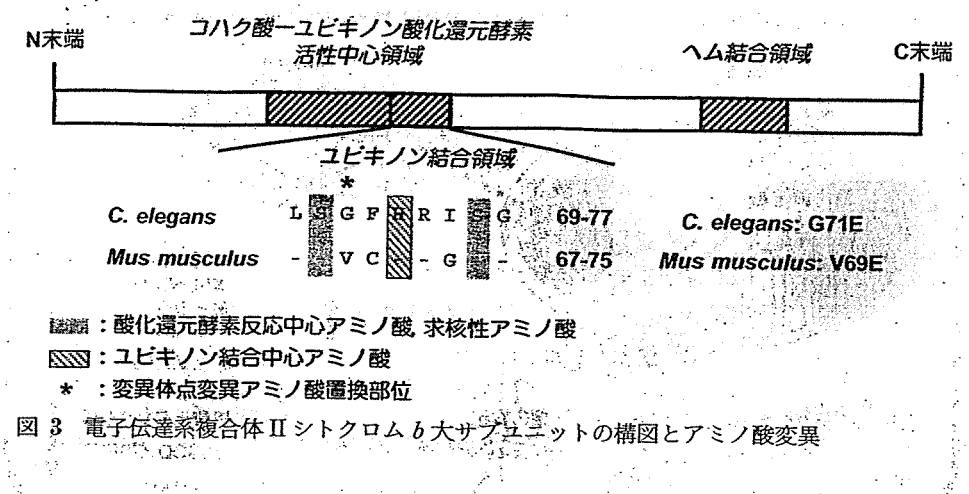

図3 電子伝達系複合体IIシトクロム *b* 大サブユニットの構図とアミノ酸変異

酸性アミノ酸へと置換する変異は，酸化還元反応に重要である求核性アミノ酸の機能阻害や，複合体IIとユビキノンとの親和性の低下を引き起こすものと示唆された．そこで，マウスSDHCアミノ酸においても，*C. elegans*，*mev-1* 変異体のアミノ酸点変異部位と同様の部位に位置する中性アミノ酸を酸性アミノ酸へ（V69E）と置換したアミノ酸（SDHC V69E）（図3）を発現する外来遺伝子（変異型 *SDHC* 遺伝子：*SDHC* T206，207A）を構築した[19]．変異型遺伝子が過剰発現した細胞株では，形態変化や過剰なアポトーシス誘導などの形質変化が確認され，致死となるものが多く観察された．そこで，この変異型 *SDHC* 遺伝子を導入したNIH3T3細胞の中から，変異型 *SDHC* 遺伝子導入による直接の影響が確認されていない細胞株（*SDHC* 遺伝子の発現量が1：1の構成的な発現となる細胞株）をSDHC E69細胞株として樹立した[19]．次項に，この細胞株の表現型解析の結果について述べる．

2) ミトコンドリア代謝および活性酸素発生量の変化

SDHC E69細胞株では，ミトコンドリア電子伝達系複合体活性のうち，複合体II-III（コハク酸-シトクロム *c* 酸化還元酵素）酵素活性が，NIH3T3細胞野生株のものと比較し約30%にまで減少していた[19]．これは *C. elegans*，*mev-1* 変異体の解析結果と一致していた．また，ATPの細胞内存在量においても *C. elegans*，*mev-1* 変異体の解析結果と同様に変化は観察されなかった[19]．この結果が，ATP産生量が変化していないことを反映した結果であるのか，またはATP消費量が低下して事実上ATP存在量が変化していないものなのかは未解明である．

さらに，複合体IIのコハク酸脱水素酵素（SDH）活性には変化が確認されないことから，複合体IIより発生した電子は複合体II-III酵素活性の低下に伴い，複合体IIIへと伝達されずに漏出していることが考えられた．これは，ミトコンドリアから発生する活性酸素産生のメカニズムに酷似する．そこで，ミトコンドリアから発生する活性酸素量を *in vitro* および *in vivo* において測定した．その結果，野生株では複合体IIの基質であるコハク酸を加えた際に活性酸素産生量の変化は確認されず，複合体III特異的な電子伝達阻害剤（QNO）を加えることにより活性酸素産生量が増加した（図4）．したがって，コハク酸を基質としたコハク酸脱水素酵素（SDH）活性により発生した電子が複合体IIから複合体IIIへと伝達され，コハク酸-シトクロム *c* 酸化還元酵素活性が正常であることを証明している．一方，SDHC E69細胞株ではコハク酸を加えることで活性酸素発生量が増加し，SDH活性により発生した電子は複合体II-III間から漏出し，ミトコンドリア内の近傍の酸素と反応し，活性酸素を過剰発生していることが示唆された（図4）．また，複合体Iの基質であるNADHを加えた際には，野生株およびSDHC E69細胞株のミトコンドリアからの活性酸素産生は確認されなかった．さらに，ユビキノン（CoQ_{10}）を過剰添加した培地で

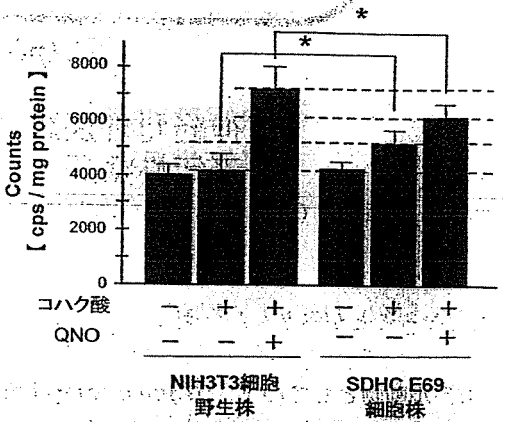

図4 *in vitro* 測定系におけるミトコンドリアからの活性酸素発生量の変化（文献14より改変）

活性酸素特異的化学発光試薬（MPEC）を用い，ミトコンドリア画分タンパク質に複合体IIの基質コハク酸（succinate）および複合体III特異的電子伝達阻害剤（QNO）を添加した際に発生した活性酸素量を測定した．＊：$p<0.05$

培養した細胞株の活性酸素発生量を測定した結果，コハク酸添加時に生じていた過剰な活性酸素発生は抑制されていた[19]．このことは，SDHC V69E タンパク質をサブユニットとした複合体IIとユビキノンとの間から漏出した電子が原因となってミトコンドリアから過剰な活性酸素が発生していることを裏付ける結果となった．また，*in vivo* での測定結果から，SDHC E69 細胞株において継代培養期間に応じてミトコンドリア内の活性酸素蓄積量が増加していることが確認された[19]．

DNPH (2,4-dinitrophenylhydrazine) 抗体を用いたカルボニル化タンパク質量測定の結果，野生株と比べ，SDHC E69 細胞株においてミトコンドリア内の活性酸素蓄積量に応じたカルボニル化タンパク質の蓄積が認められた[19]．また，DNA への酸化ストレス障害の指標である 8-OHdG (8-hydroxydeoxyguanosine, 8-oxo-2′-deoxyguanosine) の蓄積量も SDHC E69 細胞株において野生株と比べ約2倍の増加が確認された[19]．8-OHdG は DNA に突然変異を生じさせることから，6-チオグアニン (6-TG) 耐性試験による染色体 DNA 上の変異誘発有無の確認を行った〔6-TG は hypoxanthine phosphoribosyl transferase (hprt) により代謝され細胞内毒素として細胞を致死に陥れる〕．その結果，3か月間培養の SDHC E69 細胞株は野生型や1か月間培養の SDHC E69 細胞株と比べ約2倍の耐性を示し，高頻度に DNA 上に変異が生じていることが確認された[19]．さらに，2%生存下の 6-TG 濃度の培地中において，3か月間培養の SDHC E69 細胞株のみが多くのコロニーを形成した[19]．この結果は，hprt 遺伝子を含む染色体 DNA 上で高頻度に継続的な変異誘発が生じていることを裏付けている．*C. elegans*, *mev-1* 変異体においても，染色体 DNA 上への突然変異率が上昇していることが報告されていることから，複合体IIより発生した活性酸素による酸化ストレス障害が染色体 DNA 上へ及ぶことが明らかにされているが，直接的な原因となっているかどうかは未だ解明されていない．

5. SDHC E69 変異細胞株の形態変化

1) 細胞形態および細胞増殖能の変化

野生株は3か月間の培養を継続しても，紡錘状を維持した線維芽細胞様および単層培養形態を維持していた．一方，樹立後1か月間培養を継続した SDHC E69 細胞株では接着阻止現象の消失やアポトーシス小体様の多くの小顆粒が確認された（図5A）．また，コロニー形成時にはその中央部に細胞死によるものと示唆される空間が生じていた[19]．興味深いことに，樹立後凍結保存した SDHC E69 細胞株では，再度培養を開始した約2週間以降から同様の表現型が確認された．この結果は，これらの表現型が細胞内に蓄積された活性酸素に起因していることを示唆する結果である．さらに，3か月間培養後の SDHC E69 細胞株では接着阻止現象の消失やアポトーシス小体様の多くの小顆粒出現に加え，細胞形態が紡錘状から平滑状の円状形態

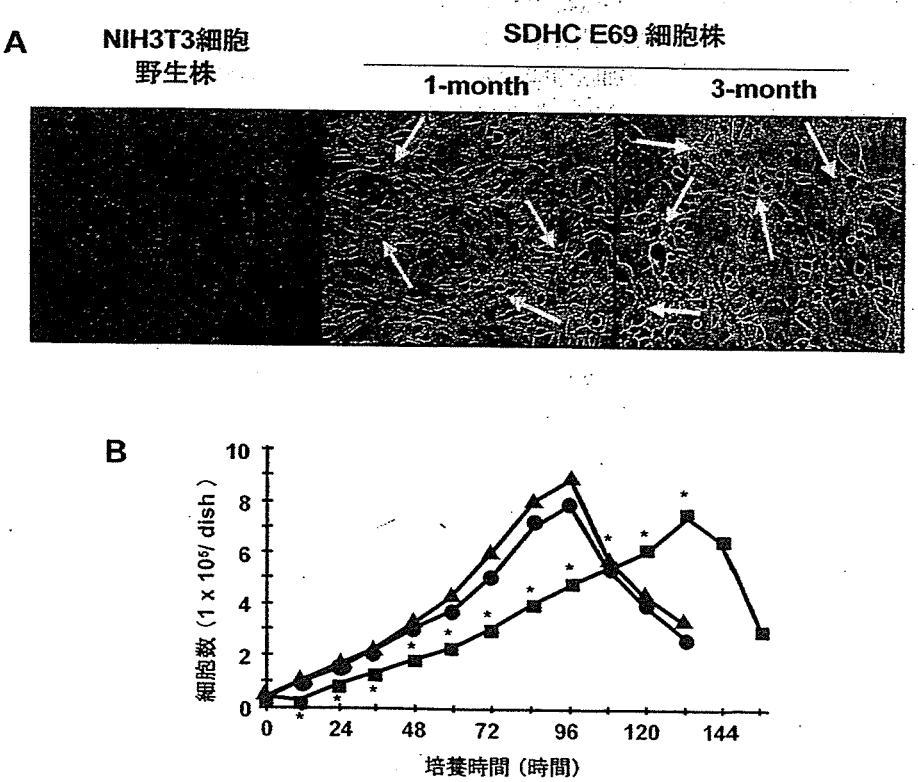

図5 細胞形態および細胞増殖能の変化
（文献14より改変）
A，3か月間の継代培養を行った野生株 NIH3T3 細胞，1か月間および3か月間の継代培養を行った SDHC E69 細胞株で形態観察を行った．黒矢印：アポトーシス様小顆粒（original magnification：100×）．B，形態観察と同様の細胞株で細胞増殖能の測定を行った．野生株 NIH3T3 細胞（●），1か月間継代培養を行った SDHC E69 細胞株（■），3か月間継代培養を行った SDHC E69 細胞株（▲）．*：$p<0.01$

へと変化し，重層培養形態が確認された（図5A）．

1か月間培養のSDHC E69細胞株では，細胞増殖速度を示す倍加時間が野生株のものと比べ1.5から2倍に延長していた（図5B）．一方，興味深いことに3か月間培養後のSDHC E69細胞株の倍加時間は野生株のものと同等にまで回復しており（図5B），細胞の形態変化に伴い細胞増殖能の有意な変化が観察された．以上の結果から，SDHC E69細胞株ではアポトーシスが誘導されており，さらに，3か月間培養のSDHC E69細胞株では形質転換を生じた結果であると示唆された．

2) SDHC E69変異細胞株の形質転換

ヌードマウスへの皮下移植実験の結果，1か月間の培養を行ったSDHC E69細胞株は野生株と比べ早期に消失することが確認された[19]．この結果は，アポトーシスを誘導していた1か月間培養のSDHC E69細胞株が，貪食されたことを示唆している．一方，3か月間の培養を行い形質転換を生じたと示唆されたSDHC E69細胞株では造腫瘍性が確認された[19]．形質転換後の細胞では足場非依存的な増殖が可能になることが知られている．そこで，軟寒天培養法による1か月間の培養中に生じる形質転換効率を測定した．その結果，1か月間培養のSDHC E69細胞株の形質転換効率は5×10^{-4} cells，3か月間培養のもので5×10^{-3} cellsであった[19]．野生株のNIH3T3細胞株の形質転換効率は1×10^{-6} cellsであると報告されていることから，SDHC E69細胞株の形質転換効率は，継代培養ごとに蓄積する活性酸素量に伴い，野生株に比べ約100から1,000倍へと増加していることが確認された[19]．

さらに，ヌードマウス皮下において造腫瘍性を示した組織の観察を行った結果，野生株の中で自然突然変異によって形質転換した細胞は移植定着後肥大化することが確認された．しかし，ミトコンドリアからの酸化ストレスにより形質転換した3か月間培養のSDHC E69細胞株は移植定着後の肥大化は確認されず，良性腫瘍の表現型が確認された（論文作成中）．この結果は，複合体IIのSDHCやSDHDサブユニットの遺伝子変異が家族性の傍神経節腫（パラガングリオーマ）などの腫瘍形成の原因になるといった報告[20]を支持する．

6. SDHC E69変異細胞株でのアポトーシス誘導

電子顕微鏡によるミトコンドリア構造の観察から，SDHC E69細胞株において，クリステの消失や膨潤化，膨大化が確認された[19]．膨大化は，おそらく野生型SDHCや変異型SDHC V69Eサブユニットを含んだミトコンドリアが正常な機能を維持するために増殖や融合を繰り返した結果であると示唆された．さらに，SDHC E69細胞株においてミトコンドリア膜電位およびミトコンドリア膜脂質量の低下が確認された[19]．これらミトコンドリアの膨潤化や膜電位の低下といった現象はアポトーシス誘導初期の表現型として知られている[21]．そこで，アポトーシス誘導の指標となるカスパーゼ3の活性測定を行った結果，SDHC E69細胞株において野生株と比較し1.6から1.8倍の上昇が認められた[19]．また同時に，DNA断片化も亢進していることが確認された[19]．以上の結果から，SDHC E69細胞株のアポトーシス小体様の顆粒出現は，ミトコンドリアの形態異常および膜電位低下によるアポトーシス誘導によるものであることが明らかとなった．従来，形質転換後のがん細胞はアポトーシス誘導の阻害により細胞分裂の無秩序化，無限増殖化が進行するとされてきた．しかし，形質転換後のSDHC E69細胞株ではアポトーシス誘導が亢進していることが明らかとなった．

今後，形質転換後のSDHC E69細胞株の詳細な解析が行われることで，パラガングリオーマ発症の分子メカニズム解明の端緒となることが期待される．

7. おわりに

我々はミトコンドリア電子伝達系複合体IIのシトクロムb大サブユニット（CYT-1，SDHC）にアミノ酸点変異（CYT-1 G71E，SDHC V69E）を挿入することで，このサブユニットとユビキノンとの親和性の低下，および求核性アミノ酸セリン残基の機能阻害を生じさせ，電子伝達系複合体IIから電子を漏出するモデル動物の作製に成功し解析を進めている．これらのモデル動物では漏出した電子が近傍の酸素と反応することでミトコンドリアから過剰な活性酸素を発生し，動物の生体内環境により近い状態での細胞内酸化ストレス負荷を生じている．

今回，新たに報告したマウス細胞株の表現型解析の結果は，ミトコンドリアから生じる過剰な活性酸素による細胞内酸化ストレスが細胞増殖能の低下を招き，その後，正常細胞株と比べ高頻度に形質転換を生じ，強度の酸化ストレス下においても細胞増殖能が正常細胞にまで回復することを明らかにした．また，今回用いた細胞株での過剰なアポトーシスの誘導は活性酸素の蓄積量とともに増加していることが確認され，形質転換後の細胞株においてもアポトーシス誘導がより強く誘起されることが明らかになった．がん細胞ではアポトーシス誘導が抑制あるいは阻害されているといった認識が強いが，今回の細胞株では正常細胞以上にアポトーシス誘導の増強が確認された．これにより，形質転換後の細胞は，腫瘍組織の増大のない良性腫瘍の形質を維持しているものと示唆された．この表現型の特性をより明確に捉えることで，ヒトでのパラガングリオーマ発症の原因解明の端緒を担うことが期待できる．今後，SDHC E69細胞株の正常細胞と形質転換細胞とを明確に区別し，ミトコンドリアからの活性酸素により活性化されるシグナ

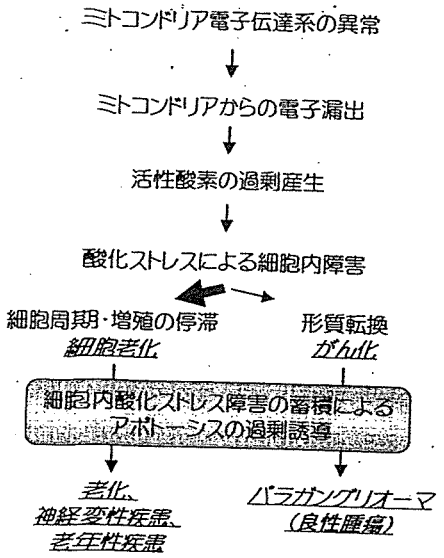

図 6 SDHC E69細胞株におけるミトコンドリアから発生した活性酸素による過剰なアポトーシス誘導と形質転換の経緯

伝達経路や形質転換のメカニズムの詳細な解析が行われることで，それぞれの細胞におけるミトコンドリアからの化ストレスの影響が明らかにされることを期待するものある．

以上の結果を生体において考察すると，ミトコンドリア子伝達系から漏出した電子は活性酸素を発生させ，大部の細胞において細胞周期の停滞あるいは細胞増殖能の停を引き起こす．また，細胞老化すなわち個体の老化を導，一部の細胞で形質転換を生じると示唆された（図6）．らに，これらの表現型を生じるなかで，細胞内に蓄積さた酸化ストレスは過剰なアポトーシス誘導を実行し細胞の低下を導く．その影響は正常な組織器官においては急な臓器萎縮を引き起こし様々な疾患の原因となり，がん織においては細胞増殖の抑制に効果を示し，そのがん組に良性腫瘍の特性を保持させているものと考えられた[6]．今後，SDHC V69E変異を適用した哺乳類におけモデル動物の解析によって，個体老化を導く細胞老化の因となる細胞周期の停滞，神経変性疾患などの老人性疾の原因となる過剰なアポトーシス誘導やパラガングリオマなどの発がん過程におけるミトコンドリア酸化ストレの関与を明らかにしていくことが期待できる．

最後に，ここに紹介した一連の研究に関わっていただいた共同研究者の方々に深く感謝申し上げます．

文　献

1) Raha, S. & Robinson, B.H. (2000) *Trends. Biochem. Sci.* **25**, 502-508
2) Yankovskaya, V., Horsefield, R., Tornroth, S., Luna-Chavez, C., Miyoshi, H., Leger, C., Byrne, B., Cecchini, G., & Iwata, S. (2003) *Science* **299**, 700-704
3) Tohyama, Y., Takano, T., & Yamamura, H. (2004) *Curr. Pharm. Des.* **10**, 835-839
4) Hongpaisan, J., Winters, C.A., & Andrews, S.B. (2004) *J. Neurosci.* **24**, 10878-10887
5) Jacobson, M.D. (1996) *Trends. Biochem. Sci.* **21**, 83-86
6) Robberecht, W. (2000) *J. Neurol.* **247**, Suppl 1 : I1-6
7) Kovacic, P. & Jacintho, J.D. (2001) *Curr. Med. Chem.* 8, 773-796
8) Ishii, N., Fujii, M., Hartman, P.S., Tsuda, M., Yasuda, K., Senoo-Matsuda, N., Yanase, S., Ayusawa, D., & Suzuki, K. (1998) *Nature* **394**, 694-697
9) Senoo-Matsuda, N., Yasuda, K., Tsuda, M., Ohkubo, T., Yoshimura, S., Nakamura, H., Hartman, P.S., & Ishii, N. (2001) *J. Biol. Chem.* **276**, 41553-41558
10) Ishii, N., Takahashi, K., Tomita, S., Keino, T., Honda, S., Yoshino, K., & Suzuki, K. (1990) *Mutat. Res.* **237**, 165-171
11) Honda, S., Ishii, N., Suzuki, K., & Matsuo, M. (1993) *J. Gerontol.* **48**, B57-61
12) Hosokawa, H., Ishii, N., Ishida, H., Ichimori, K., Nakazawa, H., & Suzuki, K. (1994) *Mech. Ageing. Dev.* **74**, 161-170
13) Senoo-Matsuda, N., Hartman, P.S., Akatsuka, A., Yoshimura, S., & Ishii, N. (2003) *J. Biol. Chem.* **278**, 22031-22036
14) 埜中征哉，後藤雄一編（1997）ミトコンドリア病，医学書院
15) Bourgeron, T., Rustin, P., Chretien, D., Birch-Machin, M., Bourgeois, M., Viegas-Pēquignot, E., Munnich, A., & Rötig, A. (1995) *Nature Genet.* **11**, 144-149
16) Reichmann, H., Florke, S., Hebenstreit, G., Schrubar, H., & Riederer, P. (1993) *J. Neurol.* **240**, 377-380
17) Haas, R.H., Nasirian, F., Nakano, K., Ward, D., Pay, M., Hill, R., & Shults, C.W. (1995) *Ann. Neurol.* **37**, 714-722
18) Tabrizi, S.J., Cleeter, M.W., Xuereb, J., Taanman, J.W., Cooper, J.M., & Schapira, A.H. (1999) *Ann. Neurol.* **45**, 25-32
19) Ishii, T., Yasuda, K., Akatsuka, A., Hino, O. Hartman, P. S., & Ishii, N. (2005) *Cancer Res.* **65**, 203-209
20) Niemann, S. & Muller, U. (2000) *Nature Genet.* **26**, 268-270
21) Mignotte, B. & Vayssiere, J.L. (1998) *Eur. J. Biochem.* **252**, 1-15

Research article

Induction of myasthenia by immunization against muscle-specific kinase

Kazuhiro Shigemoto,[1,2] Sachiho Kubo,[2] Naoki Maruyama,[2] Naohito Hato,[3] Hiroyuki Yamada,[3] Chen Jie,[4] Naoto Kobayashi,[4] Katsumi Mominoki,[5] Yasuhito Abe,[6] Norifumi Ueda,[6] and Seiji Matsuda[4]

[1]Department of Preventive Medicine, Ehime University School of Medicine, Ehime, Japan. [2]Department of Molecular Pathology, Tokyo Metropolitan Institute for Gerontology, Tokyo, Japan. [3]Department of Otolaryngology and [4]Department of Integrated Basic Medical Science, Ehime University School of Medicine, Ehime, Japan. [5]Department of Biological Resources, The Integrated Center for Science, Ehime University, Ehime, Japan. [6]Department of Molecular Pathology, Ehime University School of Medicine, Ehime, Japan.

Muscle-specific kinase (MuSK) is critical for the synaptic clustering of nicotinic acetylcholine receptors (AChRs) and plays multiple roles in the organization and maintenance of neuromuscular junctions (NMJs). MuSK is activated by agrin, which is released from motoneurons, and induces AChR clustering at the postsynaptic membrane. Although autoantibodies against the ectodomain of MuSK have been found in a proportion of patients with generalized myasthenia gravis (MG), it is unclear whether MuSK autoantibodies are the causative agent of generalized MG. In the present study, rabbits immunized with MuSK ectodomain protein manifested MG-like muscle weakness with a reduction of AChR clustering at the NMJs. The autoantibodies activated MuSK and blocked AChR clustering induced by agrin or by mediators that do not activate MuSK. Thus MuSK autoantibodies rigorously inhibit AChR clustering mediated by multiple pathways, an outcome that broadens our general comprehension of the pathogenesis of MG.

Introduction

Myasthenia gravis (MG) is an antibody-mediated autoimmune disease in which the nicotinic acetylcholine receptor (AChR) at neuromuscular junctions (NMJs) is the major autoantigen (1). AChR-specific antibodies are detected in 90% of nonimmunosuppressed patients with generalized MG. However, Hoch et al. found antibodies to a novel antigen, muscle-specific kinase (MuSK), in approximately 66% of patients with generalized MG that were lacking detectable AChR autoantibodies (seronegative MG) (2). Subsequent studies have reported MuSK antibody frequencies of 4–47.4% in MG patients seronegative for AChR antibodies (3–9). MG patients with MuSK antibodies tend to develop severe facial weakness and bulbar symptoms, including dysphagia, dysarthria, and respiratory cirsis with some atrophy of facial muscles, that are often difficult to treat effectively with immunosuppressive therapies (3, 7). The pathogenic mechanisms of MG caused by AChR antibodies are well delineated, but pathogenicity has not been demonstrated for MuSK antibodies (10). Furthermore, no reports have described the induction of MG by immunization of animals with purified MuSK protein. The present study was undertaken to explore this issue. Here we describe the development of myasthenia and reduction of AChR density in rabbits immunized with the ectodomain of MuSK. The molecular pathogenesis of MG was further investigated using an in vitro assay of AChR clustering on myotubes that was mediated by MuSK antibodies.

MuSK is an AChR-associated transmembrane protein. During development of skeletal muscle, MuSK is initially required for organizing a primary synaptic scaffold to establish the postsynaptic membrane (11, 12). Prior to muscle innervation, AChR clusters form at the central regions of muscle fibers, creating an endplate zone that is somewhat broader than that in innervated muscle (13, 14). MuSK and rapsyn, which is a 43-kDa, membrane-associated cytoplasmic protein, must be expressed before the endplate zone forms (11, 15–17). Subsequent contact of the motor-neuron growth cone with the muscle extinguishes extrasynaptic AChR clusters, resulting in a narrow, distinct endplate zone in the midmuscle that is marked by a high density of AChR clustering (13, 14). In this step, agrin released from motoneurons activates MuSK and redistributes AChR clusters to synaptic sites (13, 14, 17–20). Therefore the formation of NMJs either in the absence or presence of agrin requires the expression of MuSK at the endplate membrane.

The extracellular segment of MuSK comprises 5 distinct domains, i.e., 4 immunoglobulin-like domains and 1 cysteine-rich region (21–25). All 5 domains are conserved in *Torpedo spp*, mice, humans, rats, *Xenopus*, and chickens. MuSK exerts its multiple effects through interaction of the extracellular domains with other molecules. Transfection of MuSK$^{-/-}$ myotubes with a series of mutant MuSK constructs demonstrated that the amino-terminal immunoglobulin-like domain is required for activation by agrin (26). The extracellular domains of MuSK interact with rapsyn-AChR complexes (27, 28). Although the synaptic membrane in adult muscle appears to be macroscopically stable, in vivo studies have shown that synaptic AChRs intermingle completely over a period of approximately 4 days, and that many extrasynaptic AChRs are incorporated into the synapse at the mature NMJs (29, 30). In addition, RNA interference targeting MuSK in adult mammalian muscle in vivo induced the disassembly of postsynaptic AChR clusters, with effects ranging from fragmentation to disappearance (31). Hence the mechanisms of NMJ formation by MuSK are also likely to be important for the maintenance of AChR clusters at the NMJs.

Nonstandard abbreviations used: BTX, α-bungarotoxin; GalNAc, *N*-acetylgalactosamine; MG, myasthenia gravis; MuSK, muscle-specific kinase; MuSK-AP, chimeric protein of the MuSK ectodomain and human placental alkaline phosphatase; MuSK-Fc, chimeric protein of the MuSK ectodomain and the Fc region of human IgG1; NMJ, neuromuscular junction; VVA-B4, *Vicia villosa* agglutinin.

Conflict of interest: The authors have declared that no conflict of interest exists.

Citation for this article: *J. Clin. Invest.* 116:1016–1024 (2006). doi:10.1172/JCI21545.

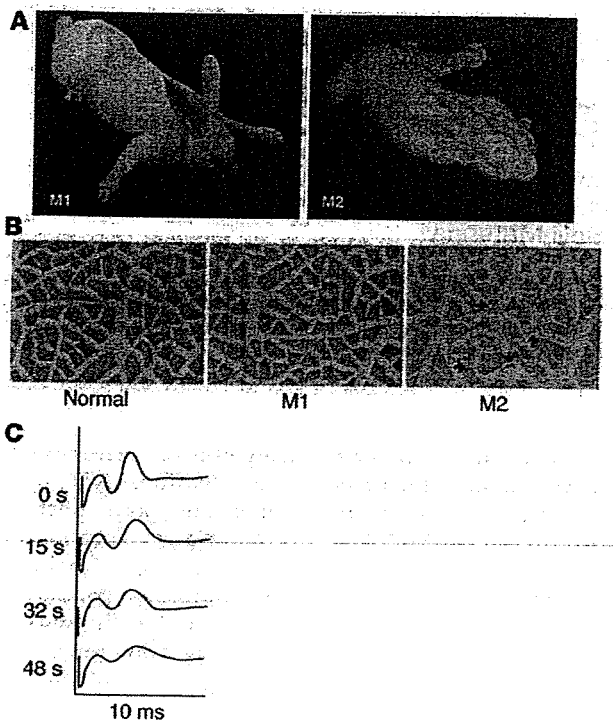

Figure 1
Rabbits manifest MG-like paresis after immunization with MuSK protein. (**A**) Two rabbits, representative of the 4 animals that showed myasthenia, manifested myasthenic weakness after immunization with the recombinant MuSK protein. After 3 injections of MuSK protein, M1 and M2 rabbits manifested flaccid weakness within 3 and 9 weeks, respectively. The M2 rabbit developed severe exhaustion with muscle weakness. (**B**) Cross sections from the soleus muscles of 2 paretic (M1 and M2) and 1 normal rabbit were stained with H&E. Muscle fibers in the M1 paretic rabbit showed only subtle changes in shape and smallness, whereas an atrophy of muscle fibers in the M2 paretic rabbit was observed as small angular fibers (arrows). Scale bar: 50 μm. (**C**) Electromyograms recorded from the M1 paretic rabbit. The retroauricular branch of the facial nerve was continuously stimulated by a constant-current stimulator, which delivered square-wave pulses of 0.1 ms at 20 Hz, and the compound muscle action potential (the second peak observed on the oscilloscope screen was recorded at the indicated time points during stimulation) showed a decremental pattern, consistent with MG.

In cultured myotubes, AChR clustering is induced by laminin-1 and the *N*-acetylgalactosamine–specific (GalNAc-specific) lectin *Vicia villosa* agglutinin (VVA-B4) without activation of MuSK (32–36). Neither the receptor nor the activation mechanisms of AChR clustering induced by agrin-independent inducers has been identified with certainty. Even so, these mechanisms may also play important roles in the maintenance of NMJs via agrin-independent pathways and in their formation, as shown by genetic studies (13, 14). The data we present herein demonstrate that MuSK autoantibodies inhibit AChR clustering by agrin itself and also by all known agrin-independent pathways.

Results

Immunization with purified MuSK protein causes flaccid weakness in rabbits. Rabbit antibodies were raised against a purified chimeric protein composed of the MuSK ectodomain and the Fc region of human IgG1 (MuSK-Fc). All of 4 recipient rabbits manifested flaccid weakness after 3 or 4 repeated injections with MuSK-Fc. Three of these rabbits developed flaccid weakness within 3 weeks after the last injection of MuSK protein, and the fourth rabbit manifested flaccid weakness 9 weeks after the third injection. Two rabbits that manifested flaccid weakness (M1 and M2 paretic rabbits) are shown in Figure 1A and Supplemental Movies 1 and 2 (supplemental material available online with this article; doi:10.1172/JCI21545DS1). Two of 4 paretic rabbits developed severe exhaustion (Figure 1A and Supplemental Movie 2; M2 paretic rabbit). Histological studies of the muscle tissues in the paretic rabbits revealed that the angular atrophic muscle fibers in the M2 paretic rabbit were intermingled with normal fibers, whereas the M1 rabbit had only subtle changes in the muscles (Figure 1B). No muscle regeneration was observed in M1 and M2 paretic rabbits (Figure 1B). The histological changes of the atrophic muscle fibers observed in the M2 paretic rabbit can result from MG, reduced mechanical activity of muscles, or cachexia (37).

These results suggest that the muscle weakness was caused by a disturbance of neuromuscular transmission due to the inhibition of MuSK functions in mature NMJs. This possibility was investigated first by an electromyographic study (38). Repetitive nerve stimulation (RNS) at a rate of 20/s in a paretic animal elicited a decremental response in compound muscle action potential (CMAP), characteristic of MG (Figure 1C). However, the CMAP in a normal rabbit did not change significantly during RNS at the same rate (data not shown). This result is consistent with the M1 rabbit having a disorder of the postsynaptic membrane as the cause of its weakness following immunization with a fragment of MuSK protein.

Reduction of AChR clustering at NMJs in paretic rabbits. Our second objective was to examine the NMJs of soleus muscles in 2 paretic (M1 and M2) and 3 normal rabbits (N1, N2, and N3) by fluorescence microscopy after applying a rhodamine-conjugated AChR antagonist, α-bungarotoxin (BTX). For semiquantitative measurement of the size and density of AChR clustering at NMJs, we determined an appropriate concentration of rhodamine-conjugated BTX by using serial dilutions of this reagent for application to frozen sections of soleus muscles (Figure 2A). A digital camera recorded images of the AChR clustering. Ten AChR clusters of NMJs were randomly chosen from the left and 10 from the right soleus muscles, after which the sizes and ODs were measured using NIH Image analysis software with the unprocessed digitized images (Supplemental Figure 1). In agreement with the electromyographic studies described above, the area and intensity of AChR fluorescence at the NMJs in both M1 and M2 paretic rabbits were significantly reduced compared with normal rabbits (area: M1, 67.9 ± 58.2 μm^2; M2, 75.0 ± 55.9 μm^2; compared with N1, 303.9 ± 125.9 μm^2; N2, 387.7 ± 163.0 μm^2; N3, 395.4 ± 150.0 μm^2; density: M1, 6219 ± 4659 OD; M2, 6889 ± 4259 OD; compared with N1, 17,770 ± 7,693 OD; N2, 23,259 ± 9,046 OD; N3, 23,870 ± 9,997 OD; Figure 2B).

Specific binding of antibodies to MuSK. As we found that muscle weakness caused by a disorder in the postsynaptic membrane was induced in rabbits via immunization with a purified MuSK protein, we next examined the ability of immune serum from paretic rabbits to react specifically with MuSK. To test whether MuSK

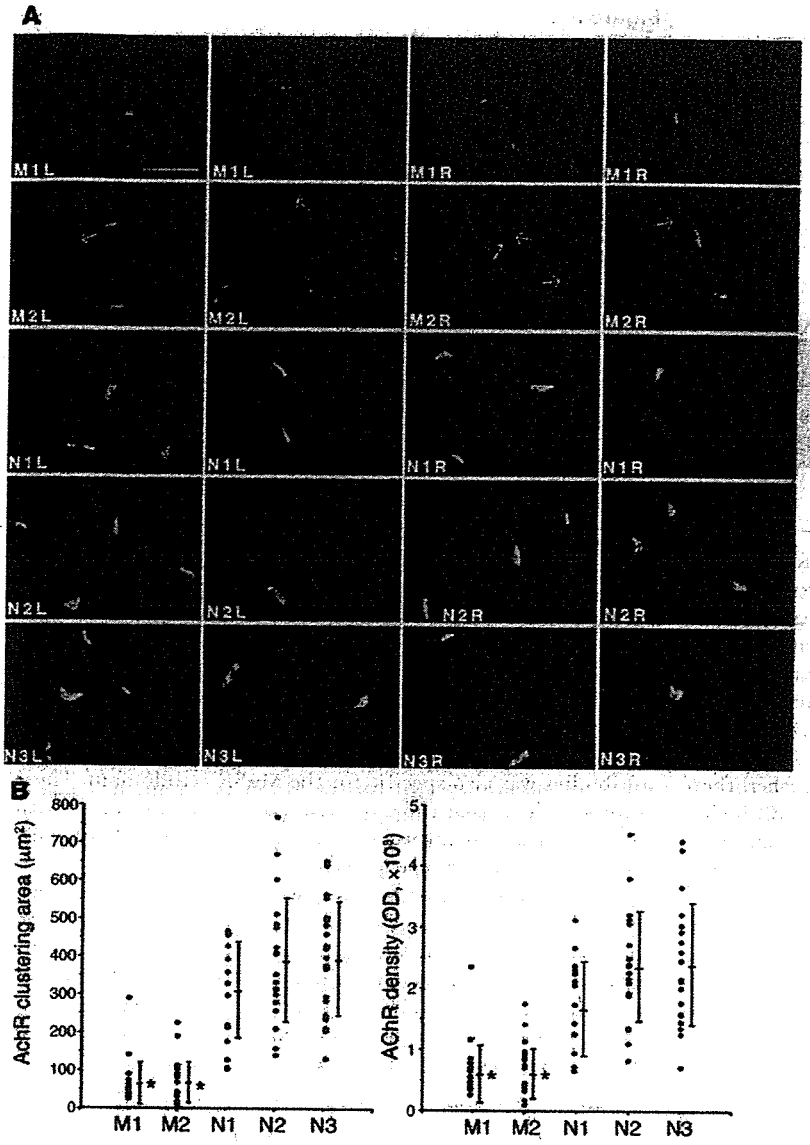

Figure 2
Reduction of the size and density of AChR clusters at the NMJs in paretic rabbits. (**A**) Cross sections from the soleus muscles of 2 paretic (M1 and M2) and 3 normal rabbits (N1, N2, and N3) were stained with 10 nM rhodamine-conjugated BTX. Bright crescents of bound BTX, indicative of endplate AChR, were smaller and less intense in the paretic rabbits' muscle fibers than in those of the normal rabbits. Arrows indicate the small angular fibers in M2 soleus muscles. L, left; R, right. Scale bar: 50 μm. (**B**) Images of 10 AChR clusters at NMJs in the right and 10 in the left soleus muscles of the paretic and normal rabbits were randomly recorded by a digital imaging camera. Quantification of the area and intensity of AChR clustering in the unprocessed images were measured using NIH Image software. Bars indicate mean ± SD. *$P < 0.01$ versus normal rabbits.

antibodies could be used to detect MuSK in Western blots, a chimeric protein that combined the MuSK ectodomain with human placental alkaline phosphatase (MuSK-AP) was transfected into COS-7 cells. As expected, proteins representing the chimeric products (~130 kDa) were secreted into the culture medium (Figure 3A). The immune serum did not react with any of the AChR subunits precipitated from a lysate of C2C12 myotubes, as determined using biotinylated BTX and streptavidin-agarose. In contrast, the AChR β subunit was detected in the same precipitate when using a monoclonal antibody (data not shown). In addition, immunohistochemical analysis showed that MuSK antibodies reacted with native MuSK molecules and colocalized with agrin-induced AChR clusters on the surfaces of differentiated C2C12 myotubes (Figure 3B). Therefore a subset of MuSK antibodies reacts specifically with MuSK molecules on the cell surface.

Activation of MuSK by autoantibodies against MuSK. Hopf and Hoch (39) reported that rabbit polyclonal antibodies against the MuSK N-terminal sequence induced the activation of MuSK and the clustering of AChR on the surfaces of C2C12 myotubes in the absence of agrin. Therefore, the effect of MuSK antibodies on the tyrosine phosphorylation of MuSK was assessed here in C2C12 cell cultures. After a 30-minute incubation with MuSK antibodies, MuSK protein was immunoprecipitated from detergent extracts of the cells by using an antiserum against its intracellular domain. Tyrosine-phosphorylated MuSK was detected in Western blots by using phosphotyrosine-specific antibodies (Figure 4A). This antibody-induced autophosphorylation was completely inhibited by absorption with an excess of MuSK-AP before the addition of MuSK antibodies to the C2C12 myotube cultures. Thus the MuSK antibodies specifically activated autophosphorylation by inducing dimerization of the MuSK molecules in the absence of agrin, as shown previously using N-terminal–specific MuSK antibodies.

The downstream cascade of MuSK also leads to tyrosine phosphorylation of the AChR β subunit (19, 40, 41). Therefore we next sought to determine whether AChRs are tyrosine phosphorylated in response to MuSK activation by the MuSK antibodies. C2C12 myotubes were exposed to biotinylated BTX to identify AChRs in phosphotyrosine immunoblots. After exposure of the myotubes to MuSK antibodies for 30 minutes, tyrosine phosphorylation of the AChR β subunit was detected at a level similar to that induced by agrin (Figure 4B). AChR phosphorylation was inhibited when the antibodies were absorbed with an excess of MuSK-AP prior to addition to cultured C2C12 myotubes, which demonstrates that the MuSK antibodies specifically induce AChR β subunit phosphorylation in the downstream cascade of MuSK. Antibodies against the intracellular domain of the MuSK protein did not phosphorylate either MuSK or the AChR β subunit (data not shown).

Inhibition of spontaneous AChR clustering by antibodies against the MuSK ectodomain. MuSK antibodies induced tyrosine phosphorylation of both MuSK and the AChR β subunit, whereas AChR clustering at the NMJs of paretic rabbits was reduced. Therefore, we next tested the ability of MuSK antibodies to stimulate AChR

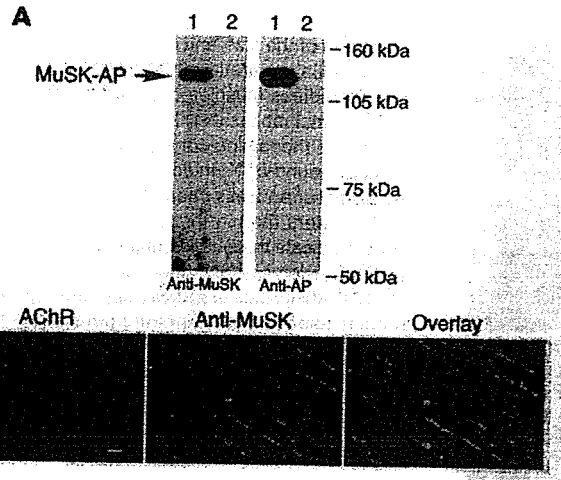

Figure 3
MuSK autoantibodies specifically bind MuSK. (**A**) Detection of secreted MuSK-AP from COS-7 cells by Western blot analysis with MuSK autoantibodies. The culture supernatants from COS-7 cells transfected with MuSK-AP (lane 1) or vector alone (lane 2) were immunoblotted with the MuSK antibodies, and the same immmunoblots were reprobed with an anti–alkaline phosphatase (anti-AP) antibody. (**B**) Specific binding of MuSK autoantibodies to MuSK in C2C12 myotubes. Myotubes were treated with agrin (1 nM for 18 h) and double labeled, first with rhodamine-conjugated BTX (left), and then with MuSK antibodies followed by fluorescein-conjugated secondary antibodies (middle). AChRs and MuSK colocalized, as shown by the overlay of red and green fluorescence (right). Green blotches are artifact. Scale bar: 20 μm.

clustering in the absence of agrin following MuSK autophosphorylation. Overnight incubation of C2C12 myotubes with MuSK antibodies in the absence of soluble agrin and labeling of AChR with rhodamine-conjugated BTX revealed that the MuSK antibodies inhibited spontaneous AChR clustering; that is, only a small number of AChR clusters formed in the myotubes in the absence of additional stimulation (Figure 5, A and B). However, AChR clustering was not blocked by antibodies against the MuSK intracellular domain (data not shown). Taken together, these results suggest that MuSK antibodies do not induce AChR clustering. Instead, they interfere with spontaneous AChR clustering by interacting with MuSK molecules in C2C12 myotubes, despite the activation of MuSK autophosphorylation.

Inhibition of agrin-induced AChR clustering by MuSK antibodies. Agrin induces clustering of AChR in C2C12 myotubes following MuSK autophosphorylation (17, 19, 20). This cascade of events is a major feature of AChR clustering at the NMJs after innervation by motoneurons (17, 36, 42, 43). In a previous study, Hoch et al. observed that the MuSK antibodies of MG patients inhibited agrin-induced AChR clustering (2), whereas we found that MuSK antibodies from paretic rabbits activated MuSK. It was therefore of interest to determine whether MuSK antibodies could interfere with agrin-induced AChR clustering in C2C12 cells as they did in spontaneous clustering. Indeed, agrin-induced clustering of AChR was strongly blocked in the presence of MuSK antibodies, whereas absorption of the antibodies with soluble MuSK-AP fusion products prevented this blocking effect (Figure 6, A and B). This result clearly demonstrates that the MuSK antibodies are responsible for inhibiting the formation of agrin-induced AChR clustering, in contrast to the N-terminal–specific MuSK antibodies, which induce AChR cluster formation in C2C2 myotubes (39).

Inhibition of agrin-independent AChR clustering by antibody against the MuSK ectodomain. Since MuSK is necessary for the signaling and effector mechanisms of agrin-independent AChR clustering at the NMJs in vivo (13, 14), we examined the ability of MuSK antibodies to inhibit AChR clustering induced by agrin-independent stimuli such as laminin-1 and VVA-B4. Incubation of laminin-1 with MuSK antibodies strongly blocked AChR clustering as well as spontaneous and agrin-induced AChR clustering (Figure 6, A and B) on C2C12 cells. After absorption of the antibodies with soluble MuSK-AP fusion products, AChR clustering in response to laminin-1 was restored (Figure 6, A and B). Thus the blocking effect was caused by these antibodies specific for the MuSK ectodomain, as was observed for agrin-induced clustering. In addition, treatment of C2C12 cells with VVA-B4 and MuSK antibodies totally blocked AChR clustering, whereas absorption of the antibodies with soluble MuSK-AP protein prevented this blocking effect (Figure 6, A and B). Therefore blocking by the antibodies was also specific for the MuSK ectodomain. These results indicate that the interaction of MuSK antibodies with MuSK molecules in myotubes leads to a reduction of AChR clustering via an agrin-independent pathway.

Blocking of neuraminidase-stimulated AChR clustering by MuSK antibodies. Treatment of C2C12 cells with neuraminidase increases both the intensity of VVA-B4 staining and the number of AChR clusters compared with spontaneous clustering (34, 43). Since AChR clustering caused by neuraminidase treatment may involve the same signaling mechanism as that induced by VVA-B4, the ability of MuSK antibodies to inhibit this response was examined. We con-

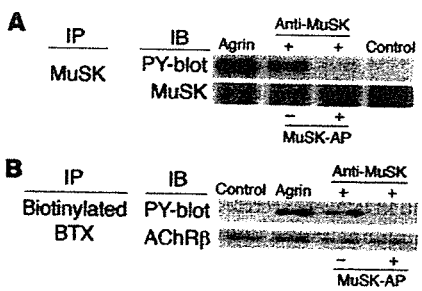

Figure 4
MuSK antibodies specifically activate MuSK and the downstream cascade. Specific phosphorylation of MuSK and AChR β subunit (AChRβ) by MuSK antibodies. C2C12 myotubes were treated with agrin or MuSK antibodies for 30 minutes and then immunoprecipitated with (**A**) MuSK antibodies or (**B**) biotinylated BTX using streptavidin-Sepharose. Immunoblots of immunoprecipitates were probed with antibodies to MuSK (**A**), AChRβ (**B**), or phosphotyrosine (PY, **A** and **B**). Both MuSK and AChRβ were phosphorylated after the treatment of agrin or MuSK antibodies. Phosphorylation of MuSK and AChRβ was inhibited by the absorption of MuSK antibodies with MuSK-AP protein.

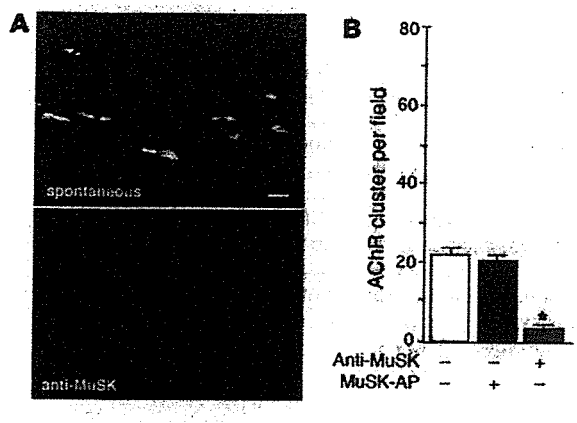

Figure 5
Inhibition of spontaneous AChR clustering by MuSK antibodies. (**A**) AChR clusters on C2C12 myotubes were stained with rhodamine-conjugated BTX with or without MuSK antibodies. Scale bar: 20 μm. (**B**) Quantification of the inhibitory activity of the MuSK antibodies showed that these antibodies provided significant inhibition of spontaneous AChR clustering (*$P < 0.01$, ANOVA). Values represent mean ± SEM of 10–15 fields for each of the 2 experiments per treatment.

firmed that neuraminidase treatment stimulated AChR clustering in C2C12 myotubes. That is, overnight incubation of C2C12 cells with 0.1 U/ml neuraminidase resulted in a 3-fold increase in the number of AChR clusters per field (Figure 7, A and B). When the C2C12 cells were incubated with MuSK antibodies and neuraminidase for 16 hours, AChR clustering was blocked efficiently, as was the clustering induced by VVA-B4. Again, absorption with MuSK-AP prevented blocking (Figure 7, A and B), which demonstrates that the inhibition of AChR clustering is caused by a direct effect of the MuSK antibodies. In summary, MuSK antibodies from paretic rabbits inhibit the AChR clustering in myotubes induced by all known agrin-independent stimuli as well as by agrin itself.

Discussion

MuSK autoantibodies are found in 4–70% of patients with generalized MG who lack detectable AChR autoantibodies (seronegative MG) (2–9); therefore, we investigated the pathogenicity of MuSK autoantibodies, as reported here. Our results demonstrate that immunization of rabbits with MuSK ectodomain protein caused myasthenic weakness and produced electromyographic findings that were compatible with a diagnosis of MG and consistent with a significant reduction of AChR clustering at NMJs. Additionally, MuSK antibodies specifically inhibited in vitro AChR clustering responses to all known stimuli, including those that act via agrin-independent pathways. Surprisingly, when applied to C2C12 muscle cells, MuSK antibodies initiated the phosphorylation of MuSK receptors and the subsequent phosphorylation of AChR in the absence of agrin, despite strongly inhibiting spontaneous AChR clustering. Furthermore, the MuSK antibodies inhibited AChR clustering induced by agrin. The possibility that MuSK antibodies contain a component that reacts with a receptor that stimulates inhibitory signals for AChR clustering seems unlikely,

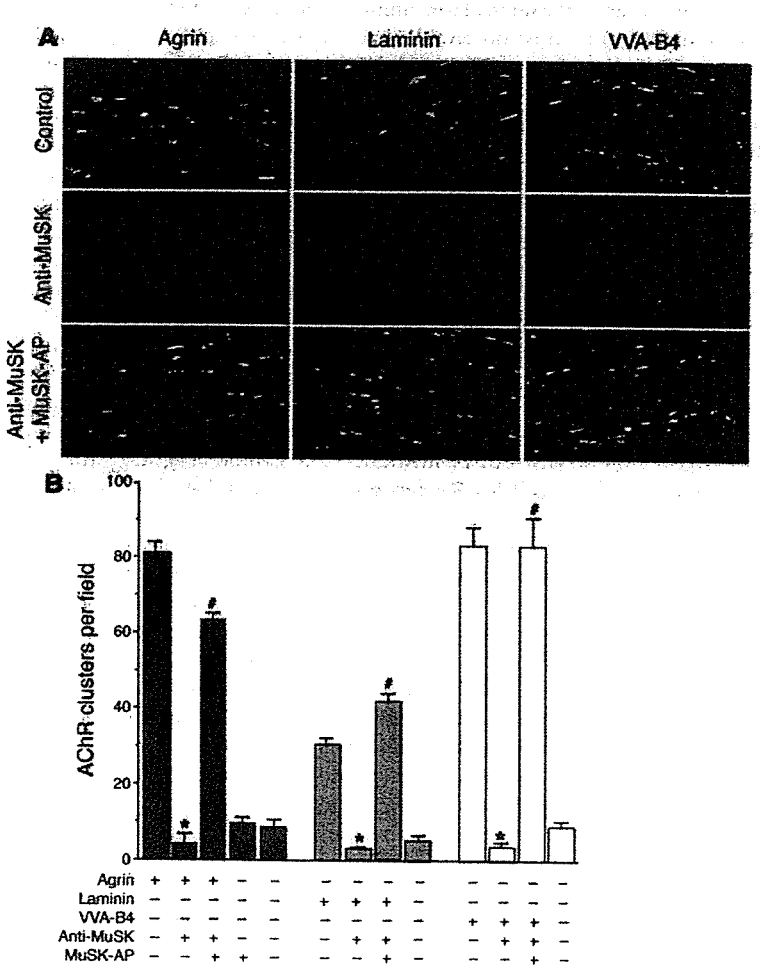

Figure 6
Inhibition of agrin-induced and agrin-independent AChR clustering by MuSK antibodies. (**A**) C2C12 cells were treated with agrin, laminin-1, or VVA-B4. AChR clusters were stained with rhodamine-conjugated BTX. AChR clustering induced by agrin, laminin-1, and VVA-B4 was inhibited in the presence of MuSK antibodies. This inhibition was blocked by absorption of the MuSK antibodies with MuSK-AP before treatment of the cells. Scale bar: 20 μm. (**B**) Quantification of the inhibitory activity of the MuSK antibodies confirmed that they significantly inhibited agrin-, laminin-1–, and VVA-B4–induced AChR clustering. Preabsorption of the MuSK antibodies with MuSK-AP significantly blocked inhibition. Values represent mean ± SEM of 10–15 fields for each of the 2 experiments per treatment. *$P < 0.01$ versus similar treatment without MuSK antibodies; #$P < 0.01$ versus similar treatment without preabsorption; ANOVA.

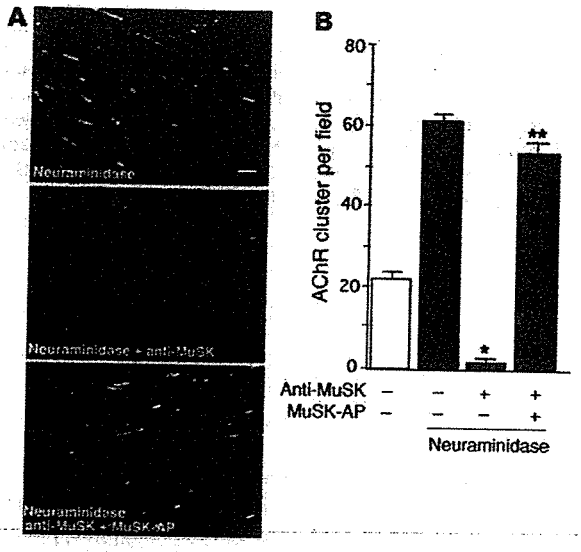

Figure 7
Inhibition of neuraminidase-induced AChR clustering by MuSK antibodies. (**A**) C2C12 cells were treated with *Clostridium perfringens* neuraminidase. AChR clusters were stained with rhodamine-conjugated BTX. AChR clustering induced by neuraminidase was inhibited in the presence of the MuSK antibodies. This inhibition was blocked by absorption of the MuSK antibodies with MuSK-AP before treatment of the cells. Scale bar: 20 μm. (**B**) Quantification of the significant inhibition of neuraminidase-induced AChR clustering by MuSK antibodies. Inhibition was significantly blocked by preabsorption of the MuSK antibodies with 6.5 nM MuSK-AP. Values represent mean ± SEM of 10–15 fields for each of the 2 experiments per treatment. $^{*}P < 0.01$ versus treatment without MuSK antibodies; $^{**}P < 0.01$ versus treatment without preabsorption; ANOVA.

since the ability of these antibodies to inhibit AChR clustering was abolished by absorption with a purified chimeric recombinant protein of MuSK. Hoch et al. have shown that plasma containing MuSK antibodies derived from patients with generalized MG who lack detectable AChR autoantibodies causes modest AChR clustering, whereas the same plasma inhibits agrin-induced AChR clustering (2). Thus, it is conceivable that a subset of MuSK antibodies expresses a strong inhibitory activity that blocks spontaneous AChR clustering, whereas other subsets of MuSK antibodies, such as those directed against the N terminus of the ectodomain, have a modest capacity to induce AChR clustering (39). An alternative possibility is that the longer incubation time with the MuSK antibodies used in the study of Hoch et al. caused the reverse effect by downregulating scaffold molecules required for AChR clustering. The effects on spontaneous clustering of MuSK antibodies reported by Hoch et al. were observed after 5 hours of incubation, whereas our analysis was carried out after a 16-hour incubation with the antibodies (2).

Neither the receptor responsible for nor the activation mechanism of AChR clustering induced on myotubes by laminin-1 is known. However, the signaling mechanisms of agrin and laminin-1 converge at a site downstream from MuSK (19, 35). Another agrin-independent stimulus, VVA-B4, recognizes terminal β-linked GalNAc residues and binds at the NMJ (33). Moreover, even in the absence of rapsyn-AChR complexes, agrin induces MuSK-based scaffolding, including the provision of binding sites for VVA-B4 on myotubes (12). Thus VVA-B4 receptors acting in concert with MuSK appear to play a key role in AChR clustering (12, 44). However, MuSK is not a receptor for VVA-B4, as demonstrated by the absence of O-linked carbohydrates providing O-linked GalNAc residues in MuSK molecules (45). Neuraminidase treatment also induces AChR clustering on myotubes by its action on terminal β-linked GalNAc residues (34). By eliminating sialic acid from glycoconjugates in the membranes, neuraminidase increases the exposure of terminal β-linked GalNAc residues that bind to the GalNAc-specific lectin VVA. We believe our observation that MuSK-specific antibodies strongly inhibited AChR clustering induced by all agrin-independent pathways as well as by agrin to be unprecedented.

Current knowledge offers several possible mechanisms for the global inhibition of this signaling pathway. Prior to innervation, MuSK is essential for organizing a primary synaptic scaffold and initiating postsynaptic membrane maturation events (11, 12, 16). These mechanisms may also be necessary for the maintenance of AChR clusters at mature NMJs, where AChR clusters undergo rapid remodeling (29, 30). Therefore, antibody to MuSK could directly prevent scaffold formation, which may be requisite for AChR clustering taking place in mature NMJs, as shown by RNA interference experiments (31). For example, the interaction of MuSK and rapsyn-AChR complexes is required for AChR clustering by agrin (11, 46). A second possible mechanism governing the inhibition of AChR clustering is an antibody-induced decrease of MuSK expression at the cell surface, which might also prevent scaffolding. In addition, the antibody could act to internalize other associated components required for agrin-dependent or agrin-independent AChR clustering. Through either mechanism, a subset of MuSK antibodies could interfere with AChR clustering even when stimulated by a different subset of MuSK antibodies and subsequently cause the extrajunctional spread of AChRs at mature NMJs.

Finally, the ability to block AChR clustering is not the sole function of MuSK antibodies, since sera containing MuSK antibodies obtained from patients with MG also inhibited agrin-dependent and agrin-independent AChR clustering on myotubes (our unpublished results). The experimental model developed here (Figure 8) is based on the use of MuSK antibodies derived from an animal whose autoimmune response impaired neuromuscular transmission. This model will facilitate further progress in resolving the pathogenic basis of MG at the molecular level and identifying other aspects of pathogenicity available to these autoantibodies in vivo.

Methods

Isolation of MuSK cDNA clones. Mouse MuSK cDNA clones were isolated by constructing a mouse C2C12 myotube cDNA library in the λ ZAPII vector (Stratagene) (47). The library was screened with a human MuSK cDNA probe amplified by reverse transcription PCR, together with a set of primers and total RNA from human muscle (Stratagene). The following primers were designed based on the sequence of the human MuSK cDNA:

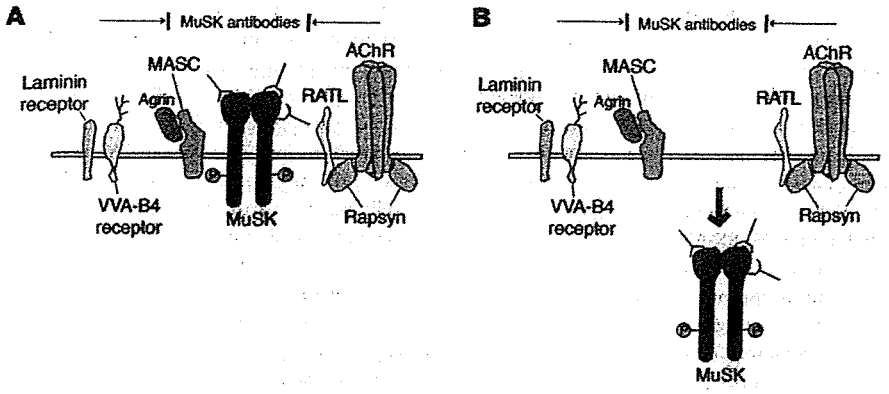

Figure 8
Models of MuSK antibody inhibition of AChR clustering on myotubes. (A) MuSK antibodies cover the ectodomain of MuSK and inhibit interactions with other scaffolding molecules required for AChR clustering, including myotube-associated component (MASC), rapsyn-associated transmembrane linker (RATL), and receptors for VVA-B4 and laminin. MASC is a hypothetical molecule that is required for agrin binding and the activation of MuSK. RATL, also a hypothetical molecule, mediates the association of rapsyn with the extracellular domain of MuSK. (B) MuSK antibodies induce the internalization of MuSK in the presence or absence of associated molecules. The lack of MuSK on the surfaces of myotubes inhibits the effects of scaffolding and AChR clustering.

5′-GTTCTCCAGAAGGAACTTCGTCCTGC-3′ and 5′-CCGTGCAGCG-CAGTAAATGCCATCATC-3′ (25). Sequences were identified using the ABI 310 DNA sequencer and BigDye Terminator v1.1 Cycle Sequencing Kit (Applied Biosystems). Sequence analysis was carried out using the GCG package of the Human Genome Center, Institute of Medical Science of the University of Tokyo.

Recombinant proteins. A MuSK-AP fusion protein was produced by amplifying the MuSK cDNA from nucleotide 2 in the 5′ untranslated region to nucleotide 1337 (GenBank/EMBL accession number AY360453) using PCR, adding terminal *Bsp*EI sites, and inserting the construct into the *Bsp*EI site of the APtag-2 vector (48). The fusion protein expression construct, which consisted of the MuSK ectodomain and the Fc region of human IgG1, was generated with the same strategy used for the alkaline phosphatase construct. The MuSK cDNA from nucleotides 2 to 1337 was amplified by PCR; an artificial splicing donor signal (GTGAGT) was added at the 3′ terminus of the cDNA, and the construct was inserted between the *Sal*I and *Spe*I sites of the vector pEF-Fc (gift from Y. Yoshihara, RIKEN Brain Science Institute, Wako, Saitama, Japan). We generated expression vectors carrying the secreted, soluble form of mouse neural agrin (C-Ag4,19; y = 4, Z = 19), using PCR to amplify the 1.5-kb C-terminal half of an alternative isoform of mouse agrin cDNA, which contains 19 amino acids at the z site, and using the first-strand cDNA of the mouse spinal cord (49). The following primers were designed based on the sequence of mouse agrin: 5′-GGGGATCCTGGCCGCTTTGGCCCAACTTGTGCAGATG-3′ and 5′-GCTCTAGAGAGAGTGGGGCAGGGTCTTAGCTC-3′ (50).

The amplified agrin cDNA, with added terminal *Bam*HI and *Xba*I sites, was inserted between the *Bam*HI and *Xba*I sites of the pSecTag vector (Invitrogen Corp.), which contains the ER signal sequence of the mouse Igκ gene (47) and a myc/his-tag sequence at the 3′ site. COS-7 cells were transfected by using Fugene-6 reagent (Roche Molecular Biochemicals) according to the manufacturer's instructions. The secreted recombinant agrin (C-Ag4,19) was concentrated with centrifugal filter devices (Millipore), and the secreted recombinant MuSK-AP and MuSK-Fc proteins were purified by using alkaline phosphatase monoclonal antibodies coupled to agarose (Sigma-Aldrich) and protein A-Sepharose (Amersham Biosciences), respectively, by standard methods (48). Agrin protein was purified from the supernatant of transfected COS-7 cells in a Sephadex G-200 column (Amersham Biosciences). Peak fractions that contained agrin were identified by Western blot analysis with anti-myc antibodies (Invitrogen Corp.), then pooled and concentrated. The purity of the recombinant proteins was determined by SDS-PAGE with silver staining. The concentration of recombinant proteins was determined by using the BCA Protein Assay kit (Pierce Biotechnology) with BSA as the standard. The relative band intensities for MuSK-AP, MuSK-Fc, agrin (z = 19), and known amounts of BSA were compared on Coomassie-stained gels as an independent measure.

Animal experiments and antibodies. The Ehime University Animal Care and Use Committee approved all of the procedures used in the animal experiments. Antiserum against the MuSK ectodomain (the MuSK antibodies) was raised by repeatedly injecting New Zealand White rabbits with 100–400 μg of protein A-Sepharose–purified MuSK-Fc. Three of the 4 injected rabbits manifested fatigable muscle weakness after 3 rounds of immunization. One rabbit developed the symptoms after the fourth round of immunization. Electromyograms were recorded from a paretic rabbit and a normal rabbit. The retroauricular branch of the facial nerve was stimulated at 20 Hz, and records were taken from the retroauricular muscle using Synax 1100 (NEC). Polyclonal antisera against the C terminus of the intracellular domain of the MuSK protein were obtained from rabbits injected with a synthetic peptide (CSIHRILQRMCERAEGTVGV). These rabbits remained healthy even after immunization. The specificity of the antiserum was confirmed by Western blot analysis using a lysate of COS-7 cells that were transfected with an expression construct of receptor-type MuSK cDNA. The IgG fraction of the MuSK antiserum was purified by standard methods using protein A-Sepharose (Amersham Biosciences). The concentration of purified IgG was determined with the BCA Protein Assay Kit (Pierce Biotechnology). Normal and paretic rabbits were anesthetized with sodium pentobarbital (Abbott Laboratories; 60 mg/kg, i.p.) and perfused transcardially with 100 ml of saline, followed by 800 ml of a fixative solution that contained 4% paraformaldehyde in 0.1 M phosphate buffer (pH 7.4). After perfusion, the middle portions of the soleus muscles were removed and immersed in the same fixative at 4°C for 24 hours. Cross sections from the soleus muscles of paretic and normal rabbits were stained with H&E for the histological studies and stained with 10 nM rhodamine-conjugated BTX (Invitrogen Corp.) for semi-quantitative measurement of the size and density of AChR clustering at NMJs. AChR clustering was examined at ×400 magnification using a fluorescence microscope (Olympus), and representative images of AChR clusters in random fields were taken with a digital camera (DP70; Olympus). With the unprocessed images, the area and OD of AChR clustering were measured using the Density Slice Command in NIH image analysis software (version 1.62; http://rsb.info.nih.gov/nih-image).

Muscle cell culture. The C2C12 cell line was obtained from the American Type Culture Collection and used for 3–5 passages. Cells were cultured in 6-well plates as myoblasts in DMEM that contained 10% FCS. When the cells reached confluence, myotube formation was induced by replacing the medium with DMEM that contained 2% horse serum. The cells were incubated for 3–4 days, with fresh medium exchange every day, until full differentiation into multinucleated myotubes was observed morphologically.

AChR clustering assay and immunocytochemical staining. AChR clustering was assayed by growing C2C12 myotubes in 6-well plates and then treating them for 16 hours with 1 nM agrin (C-Ag4,19), 40 nM laminin-1 (Kouken), 25 μg/ml VVA-B4 (Sigma-Aldrich), or 0.1 U/ml *Clostridium perfringens* neuraminidase (Sigma-Aldrich) with or without 10 μg/ml purified MuSK antibodies. The optimal dose of each inducer or MuSK antibodies required for maximal AChR clustering or inhibition, respectively, was determined. Inhibition was blocked by absorption of MuSK antibodies with 6.5 nM MuSK-AP before the cells were treated. The optimal dose of MuSK-AP for neutralization of the MuSK antibodies in the inhibition of AChR clustering assay was determined by serially diluting MuSK-AP protein premixed with antibodies at room temperature, followed by treating the C2C12 myotubes with the mixture. AChR clustering was visualized after incubation with 40 nM rhodamine-conjugated BTX (Invitrogen Corp.) in fusion medium for 1 hour at 37°C before fixation. The cells were fixed in 4% paraformaldehyde for 10 minutes at room temperature. MuSK on the myotubes was then stained using the MuSK antibodies. The myotubes were incubated with the antibodies and rhodamine-conjugated BTX for 1 hour at 37°C, rinsed, and treated with fluorescein-conjugated goat anti-mouse antibodies (BioSource International) for 1 hour at 37°C. The cells were fixed in 4% paraformaldehyde for 10 minutes at room temperature and then mounted using the SlowFade Antifade Kit (Invitrogen Corp.). The myotubes were examined at ×200 magnification using a fluorescence microscope (Olympus), and photographs of representative images of AChR clusters in random fields were taken using PRESTO NEOPAN400 (Fuji Photo Film Co. Ltd.). The numbers of AChR clusters in the photographs were then counted.

Precipitation assay and immunoblot analysis. Tyrosine phosphorylation of MuSK and AChRs induced by agrin or the antibodies was analyzed by treating C2C12 myotubes with either 1 nM agrin or 1 μg MuSK antibodies (purified by protein A-Sepharose) for 30 minutes with or without 3 nM MuSK-AP. As a control, cells were treated for 30 minutes with antibodies against the C terminus of the intracellular domain of MuSK (purified by protein A-Sepharose) at a concentration of 1 μg/ml. Cultured cells were lysed and solubilized in a protease inhibitor cocktail (Complete EDTA-free; Roche Molecular Biochemicals) with 2 mM sodium orthovanadate. The extracts were immunoprecipitated with antibodies to MuSK, and the resulting precipitates were immunoblotted with a mixture of the anti-phosphotyrosine antibodies 4G10 (Upstate USA Inc.) and PY20 (Chemicon International). MuSK was detected by stripping the blots and then reprobing them with the MuSK antibodies. Tyrosine-phosphorylated AChRs were detected by treating the cells with 120 nM biotinylated BTX (Invitrogen Corp.) for 1 hour at 4°C. The cells were then washed with cold phosphate-buffered saline, followed by lysis and precipitation with streptavidin-coupled agarose beads (Sigma-Aldrich). Phosphotyrosine immunoblotting was performed as described above. AChRs were detected by stripping the blots and then reprobing them for the AChR β subunit using a monoclonal antibody (mAb 124; kindly provided by J.M. Lindstrom, University of Pennsylvania, Philadelphia, Pennsylvania, USA) (51).

Statistics. ANOVA was used to analyze the significance of differences between experimental groups. *P* values less than 0.01 were considered statistically significant.

Acknowledgments

We thank P. Minick for excellent editorial assistance. This study was supported in part by a grant-in-aid for Scientific Research from the Ministry of Education, Science, and Culture, Japan, and a grant from the Health Science Research Grants for Comprehensive Research on Aging and Health from the Ministry of Health, Labor, and Welfare, Japan. We are also grateful to the staff of the Integrated Center for Science of Ehime University for assistance with the animal care and sequence analysis.

Received for publication March 10, 2004, and accepted in revised form February 7, 2006.

Address correspondence to: Kazuhiro Shigemoto, Department of Preventive Medicine, Ehime University School of Medicine, Sitsukawa, To-on city, Ehime 791-0295, Japan. Phone: 81-89-960-5278; Fax: 81-89-960-5279; E-mail: shigemot@m.ehime-u.ac.jp.

1. Lindstrom, J.M., Lennon, V.A., Seybold, M.E., and Whittingham, S. 1976. Experimental autoimmune myasthenia gravis and myasthenia gravis: biochemical and immunochemical aspects. *Ann. N. Y. Acad. Sci.* **274**:254–274.
2. Hoch, W., et al. 2001. Auto-antibodies to the receptor tyrosine kinase MuSK in patients with myasthenia gravis without acetylcholine receptor antibodies. *Nat. Med.* **7**:365–368.
3. Evoli, A., et al. 2003. Clinical correlates with anti-MuSK antibodies in generalized seronegative myasthenia gravis. *Brain.* **126**:2304–2311.
4. McConville, J., et al. 2004. Detection and characterization of MuSK antibodies in seronegative myasthenia gravis. *Ann. Neurol.* **55**:580–584.
5. Ohta, K., et al. 2004. MuSK antibodies in AChR Ab-seropositive MG vs AChR Ab-seronegative MG. *Neurology.* **62**:2132–2133.
6. Ohta, K., et al. 2005. MuSK Ab described in seropositive MG sera found to be Ab to alkaline phosphatase. *Neurology.* **65**:1988.
7. Sanders, D.B., El-Salem, K., Massey, J.M., McConville, J., and Vincent, A. 2003. Clinical aspects of MuSK antibody positive seronegative MG. *Neurology.* **60**:1978–1980.
8. Yeh, J.H., Chen, W.H., Chiu, H.C., and Vincent, A. 2004. Low frequency of MuSK antibody in generalized seronegative myasthenia gravis among Chinese. *Neurology.* **62**:2131–2132.
9. Zhou, L., et al. 2004. Clinical comparison of muscle-specific tyrosine kinase (MuSK) antibody-positive and -negative myasthenic patients. *Muscle Nerve.* **30**:55–60.
10. Lindstrom, J. 2004. Is "seronegative" MG explained by autoantibodies to MuSK? *Neurology.* **62**:1920–1921.
11. Apel, E.D., Glass, D.J., Moscoso, L.M., Yancopoulos, G.D., and Sanes, J.R. 1997. Rapsyn is required for MuSK signaling and recruits synaptic components to a MuSK-containing scaffold. *Neuron.* **18**:623–635.
12. Marangi, P.A., et al. 2001. Acetylcholine receptors are required for agrin-induced clustering of postsynaptic proteins. *EMBO J.* **20**:7060–7073.
13. Lin, W., et al. 2001. Distinct roles of nerve and muscle in postsynaptic differentiation of the neuromuscular synapse. *Nature.* **410**:1057–1064.
14. Yang, X., et al. 2001. Patterning of muscle acetylcholine receptor gene expression in the absence of motor innervation. *Neuron.* **30**:399–410.
15. DeChiara, T.M., et al. 1996. The receptor tyrosine kinase MuSK is required for neuromuscular junction formation in vivo. *Cell.* **85**:501–512.
16. Gautam, M., et al. 1995. Failure of postsynaptic specialization to develop at neuromuscular junctions of rapsyn-deficient mice. *Nature.* **377**:232–236.
17. Glass, D.J., et al. 1996. Agrin acts via a MuSK receptor complex. *Cell.* **85**:513–523.
18. Cohen, I., Rimer, M., Lomo, T., and McMahan, U.J. 1997. Agrin-induced postsynaptic-like apparatus in skeletal muscle fibers in vivo. *Mol. Cell. Neurosci.* **9**:237–253.
19. Ferns, M., Deiner, M., and Hall, Z. 1996. Agrin-induced acetylcholine receptor clustering in mammalian muscle requires tyrosine phosphorylation. *J. Cell Biol.* **132**:937–944.
20. Ruegg, M.A., et al. 1992. The agrin gene codes for a family of basal lamina proteins that differ in function and distribution. *Neuron.* **8**:691–699.
21. Fu, A.K., et al. 1999. Xenopus muscle-specific kinase: molecular cloning and prominent expression in neural tissues during early embryonic development. *Eur. J. Neurosci.* **11**:373–382.
22. Ganju, P., Walls, E., Brennan, J., and Reith, A.D. 1995. Cloning and developmental expression of Nsk2, a novel receptor tyrosine kinase implicated in skeletal myogenesis. *Oncogene.* **11**:281–290.
23. Ip, F.C., et al. 2000. Cloning and characterization of muscle-specific kinase in chicken. *Mol. Cell. Neurosci.* **16**:661–673.
24. Jennings, C.G., Dyer, S.M., and Burden, S.J. 1993. Muscle-specific trk-related receptor with a kringle domain defines a distinct class of receptor tyrosine kinases. *Proc. Natl. Acad. Sci. U. S. A.* **90**:2895–2899.
25. Valenzuela, D.M., et al. 1995. Receptor tyrosine kinase specific for the skeletal muscle lineage: expression in embryonic muscle, at the neuromuscular junction, and after injury. *Neuron.* **15**:573–584.
26. Zhou, H., Glass, D.J., Yancopoulos, G.D., and Sanes, J.R. 1999. Distinct domains of MuSK mediate its abilities to induce and to associate with postsynaptic specializations. *J. Cell Biol.* **146**:1133–1146.
27. Glass, D.J., et al. 1997. Kinase domain of the muscle-specific receptor tyrosine kinase (MuSK) is sufficient

for phosphorylation but not clustering of acetylcholine receptors: required role for the MuSK ectodomain? *Proc. Natl. Acad. Sci. U. S. A.* **94**:8848–8853.
28. Jones, G., Moore, C., Hashemolhosseini, S., and Brenner, H.R. 1999. Constitutively active MuSK is clustered in the absence of agrin and induces ectopic postsynaptic-like membranes in skeletal muscle fibers. *J. Neurosci.* **19**:3376–3383.
29. Akaaboune, M., Culican, S.M., Turney, S.G., and Lichtman, J.W. 1999. Rapid and reversible effects of activity on acetylcholine receptor density at the neuromuscular junction in vivo. *Science.* **286**:503–507.
30. Akaaboune, M., Grady, R.M., Turney, S., Sanes, J.R., and Lichtman, J.W. 2002. Neurotransmitter receptor dynamics studied in vivo by reversible photo-unbinding of fluorescent ligands. *Neuron.* **34**:865–876.
31. Kong, X.C., Barzaghi, P., and Ruegg, M.A. 2004. Inhibition of synapse assembly in mammalian muscle in vivo by RNA interference. *EMBO Rep.* **5**:183–188.
32. Sugiyama, J.E., Glass, D.J., Yancopoulos, G.D., and Hall, Z.W. 1997. Laminin-induced acetylcholine receptor clustering: an alternative pathway. *J. Cell Biol.* **139**:181–191.
33. Sanes, J.R., and Cheney, J.M. 1982. Lectin binding reveals a synapse-specific carbohydrate in skeletal muscle. *Nature.* **300**:646–647.
34. Martin, P.T., and Sanes, J.R. 1995. Role for a synapse-specific carbohydrate in agrin-induced clustering of acetylcholine receptors. *Neuron.* **14**:743–754.
35. Marangi, P.A., Wieland, S.T., and Fuhrer, C. 2002. Laminin-1 redistributes postsynaptic proteins and requires rapsyn, tyrosine phosphorylation, and Src and Fyn to stably cluster acetylcholine receptors. *J. Cell Biol.* **157**:883–895.
36. Gautam, M., DeChiara, T.M., Glass, D.J., Yancopoulos, G.D., and Sanes, J.R. 1999. Distinct phenotypes of mutant mice lacking agrin, MuSK, or rapsyn. *Brain Res. Dev. Brain Res.* **114**:171–178.
37. Carpenter, S., and Karpati, G. 1984. Major general pathological reactions and their consequences on skeletal muslce cells. In *Pathology of skeletal muscle.* S. Carpenter and G. Karpati, editors. Churchill Livingstone Inc. New York, New York, USA. 63–139.
38. Patrick, J., and Lindstrom, J. 1973. Autoimmune response to acetylcholine receptor. *Science.* **180**:871–872.
39. Hopf, C., and Hoch, W. 1998. Dimerization of the muscle-specific kinase induces tyrosine phosphorylation of acetylcholine receptors and their aggregation on the surface of myotubes. *J. Biol. Chem.* **273**:6467–6473.
40. Mittaud, P., Marangi, P.A., Erb-Vogtli, S., and Fuhrer, C. 2001. Agrin-induced activation of acetylcholine receptor-bound Src family kinases requires Rapsyn and correlates with acetylcholine receptor clustering. *J. Biol. Chem.* **276**:14505–14513.
41. Wallace, B.G. 1994. Staurosporine inhibits agrin-induced acetylcholine receptor phosphorylation and aggregation. *J. Cell Biol.* **125**:661–668.
42. Burgess, R.W., Nguyen, Q.T., Son, Y.J., Lichtman, J.W., and Sanes, J.R. 1999. Alternatively spliced isoforms of nerve- and muscle-derived agrin: their roles at the neuromuscular junction. *Neuron.* **23**:33–44.
43. Gautam, M., et al. 1996. Defective neuromuscular synaptogenesis in agrin-deficient mutant mice. *Cell.* **85**:525–535.
44. McDearmon, E.L., Combs, A.C., and Ervasti, J.M. 2001. Differential Vicia villosa agglutinin reactivity identifies three distinct dystroglycan complexes in skeletal muscle. *J. Biol. Chem.* **276**:35078–35086.
45. Watty, A., and Burden, S.J. 2002. MuSK glycosylation restrains MuSK activation and acetylcholine receptor clustering. *J. Biol. Chem.* **277**:50457–50462.
46. Gillespie, S.K., Balasubramanian, S., Fung, E.T., and Huganir, R.L. 1996. Rapsyn clusters and activates the synapse-specific receptor tyrosine kinase MuSK. *Neuron.* **16**:953–962.
47. Shigemoto, K., et al. 2000. Identification and characterization of 5′ extension of mammalian agrin cDNA, the exons and the promoter sequences. *Biochim. Biophys. Acta.* **1494**:170–174.
48. Cheng, H.J., Nakamoto, M., Bergemann, A.D., and Flanagan, J.G. 1995. Complementary gradients in expression and binding of ELF-1 and Mek4 in development of the topographic retinotectal projection map. *Cell.* **82**:371–381.
49. Tsim, K.W., Ruegg, M.A., Escher, G., Kroger, S., and McMahan, U.J. 1992. cDNA that encodes active agrin. *Neuron.* **8**:677–689.
50. Rupp, F., et al. 1992. Structure and chromosomal localization of the mammalian agrin gene. *J. Neurosci.* **12**:3535–3544.
51. Tzartos, S.J., Rand, D.E., Einarson, B.L., and Lindstrom, J.M. 1981. Mapping of surface structures of electrophorus acetylcholine receptor using monoclonal antibodies. *J. Biol. Chem.* **256**:8635–8645.

Senescence marker protein 30 functions as gluconolactonase in L-ascorbic acid biosynthesis, and its knockout mice are prone to scurvy

Yoshitaka Kondo, Yoko Inai, Yasunori Sato, Setsuko Handa, Sachiho Kubo, Kentaro Shimokado, Sataro Goto, Morimitsu Nishikimi, Naoki Maruyama, and Akihito Ishigami

PNAS 2006;103;5723-5728; originally published online Apr 3, 2006;
doi:10.1073/pnas.0511225103

Senescence marker protein 30 functions as gluconolactonase in L-ascorbic acid biosynthesis, and its knockout mice are prone to scurvy

Yoshitaka Kondo*†‡, Yoko Inai‡§, Yasunori Sato*‡¶, Setsuko Handa*, Sachiho Kubo*, Kentaro Shimokado†, Sataro Goto¶, Morimitsu Nishikimi§‖, Naoki Maruyama*, and Akihito Ishigami*,**

*Department of Molecular Pathology, Tokyo Metropolitan Institute of Gerontology, Tokyo 173-0015, Japan; †Vascular Medicine and Geriatrics, Tokyo Medical and Dental University, Tokyo 113-8510, Japan; §Department of Biochemistry, Wakayama Medical University, Wakayama 641-0012, Japan; and ¶Department of Biochemistry, Toho University, Chiba 274-8510, Japan

Edited by John E. Halver, University of Washington, Seattle, WA, and approved February 27, 2006 (received for review December 30, 2005)

We originally identified senescence marker protein 30 (SMP30) as a distinctive protein whose expression decreases in an androgen-independent manner with aging. Here, we report its sequence homology found in two kinds of bacterial gluconolactonases (GNLs) by using the BLAST search. Then, through a biochemical study, we identify SMP30 as the lactone-hydrolyzing enzyme GNL of animal species. SMP30 purified from the rat liver had lactonase activity toward various aldonolactones, such as D- and L-glucono-δ-lactone, D- and L-gulono-γ-lactone, and D- and L-galactono-γ-lactone, with a requirement for Zn^{2+} or Mn^{2+} as a cofactor. Furthermore, in SMP30 knockout mice, no GNL activity was detectable in the liver. Thus, we conclude that SMP30 is a unique GNL in the liver. The lactonase reaction with L-gulono-γ-lactone is the penultimate step in L-ascorbic acid (AA) biosynthesis, and the essential role of SMP30 in this synthetic process was verified here by a nutritional study using SMP30 knockout mice. These knockout mice ($n = 6$), fed a vitamin C-deficient diet, did not thrive; i.e., they displayed symptoms of scurvy such as bone fracture and rachitic rosary and then died by 135 days after the start of receiving the deficient diet. The AA levels in their livers and kidneys at the time of death were <1.6% of those in WT control mice. In addition, by using the SMP30 knockout mouse, we demonstrate that the alternative pathway of AA synthesis involving D-glucurono-γ-lactone operates *in vivo*, although its flux is fairly small.

aging | osteogenic disorder | vitamin C

Senescence marker protein 30 (SMP30) is a 34-kDa protein whose tissue levels in the liver, kidney, and lung decrease with aging (1, 2). To examine the physiological function of SMP30, we established SMP30 knockout mice (3) and found that they were viable and fertile, although they were lower in body weight and shorter in life span than WT mice (4). Their livers were also far more susceptible to TNF-α- and Fas-mediated apoptosis than those of WT mice, indicating that SMP30 may act to protect cells from apoptosis (3). The livers of SMP30 knockout mice showed abnormal accumulations of triglycerides, cholesterol, and phospholipids (4). In addition, the lungs of these knockout mice had enlarged alveolar airspaces during their first to sixth month of life (2). However, the molecular mechanism of SMP30 function has remained obscure.

Recently, we reported that SMP30 acts as a hydrolase for diisopropyl phosphorofluoridate (5), a compound resembling chemical warfare nerve agents such as sarine, soman, and tabun. However, a physiological substrate for SMP30 must be present, because this compound is an artificial chemical. Our recent search for amino acid sequences resembling SMP30 was accomplished by using the BLAST program, which revealed that rat SMP30 is homologous with gluconolactonase (GNL) [EC 3.1.1.17], a lactone-hydrolyzing enzyme, of *Nostoc punctiforme* and *Zymomonas mobilis* (6). Therefore, we suspected that SMP30 is a GNL of animal species. In mammalian metabolism, GNL is involved in L-ascorbic acid (AA) biosynthesis, catalyzing the lactonization of L-gulonic acid, the reverse reaction of lactone hydrolysis (7). The product L-gulono-γ-lactone is oxidized to AA (8–10). In this study, to further investigate the identity of SMP30, we have unequivocally proven that it is a GNL. Purified rat liver SMP30 had GNL activity, as did a recombinant rat SMP30 produced in *Escherichia coli*. Furthermore, SMP30 knockout mice developed symptoms of scurvy when fed a vitamin C-deficient diet, verifying the pivotal role of SMP30 in AA biosynthesis.

Results

Identification of SMP30 as a GNL. Comparisons of the amino acid sequence of rat SMP30 by means of the BLAST program revealed that this protein was homologous with two kinds of bacterial GNLs. The total amino acid sequence of rat SMP30 (299 aa) shares 32% homology with that of *N. punctiforme* GNL (292 aa) (Fig. 1*A*), and a part of the amino acid sequence of rat SMP30 (222 aa, residues 9–230) shares 26% homology with that of *Z. mobilis* GNL (247 aa, residues 67–313) (Fig. 1*B*). Therefore, we speculated that the protein characterized previously as SMP30 in several animals is a GNL. For substantiation, we took this protein from the rat liver and purified it to apparent homogeneity as described in ref. 5. The elution profile of SMP30 obtained with Sephacryl S-200 HR chromatography, which was the final step of the purification process, coincided well with that of GNL activity (Fig. 7*A*, which is published as supporting information on the PNAS web site), clearly indicating an overlap between them. Conversely, GNL from the rat liver was purified to near homogeneity by a previously reported method (11). The resulting preparation gave a positive band on Western blot analysis by using anti-rat SMP30 antibody (Fig. 7*B*). Moreover, the main band of a gel processed by SDS/PAGE was subjected to sequence analysis after in-gel digestion with trypsin, and the amino acid sequence of its peptide (YFAGTMAEETAP) proved to be an exact match with an internal sequence (amino acid residues 113–124) of rat SMP30.

Expression of Catalytically Active Recombinant SMP30. The identity of SMP30 as a GNL was further confirmed by expressing a rat

Conflict of interest statement: No conflicts declared.

This paper was submitted directly (Track II) to the PNAS office.

Abbreviations: AA, L-ascorbic acid; BMD, bone mineral density; GNL, gluconolactonase; MBP, maltose-binding protein; SMP30, senescence marker protein 30.

‡Y.K., Y.I., and Y.S. contributed equally to this work.

‖To whom correspondence may be addressed. E-mail: nishikim@wakayama-med.ac.jp.

**To whom correspondence may be addressed at: Department of Molecular Pathology, Tokyo Metropolitan Institute of Gerontology, 35-2 Sakae-cho, Itabashi-ku, Tokyo 173-0015, Japan. E-mail: ishigami@tmig.or.jp.

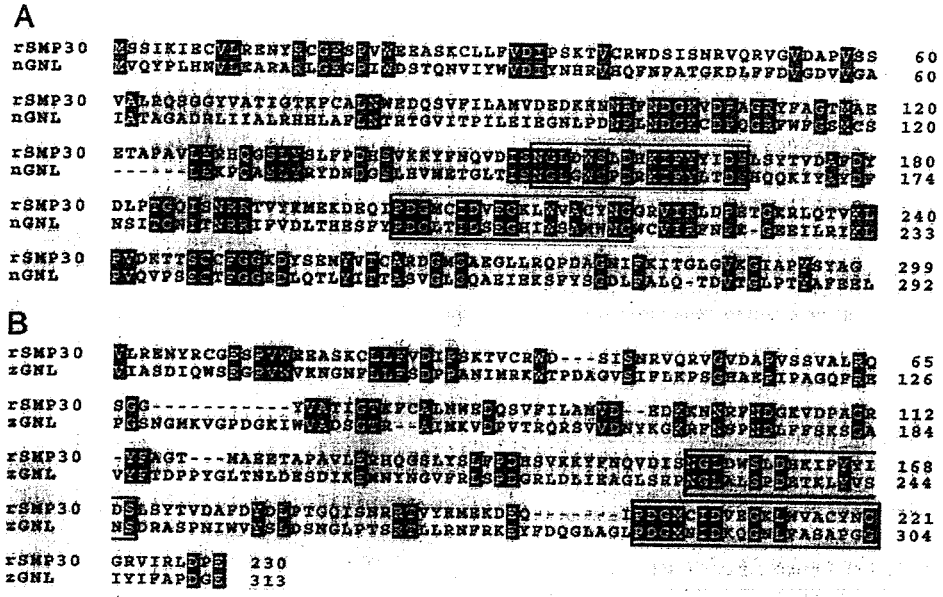

Fig. 1. Alignment of the amino acid sequences of rat SMP30 (rSMP30), *Nostoc* GNL (nGNL), and *Zymomonas* GNL (zGNL). (*A*) rSMP30 [National Center for Biotechnology Information (NCBI) accession no. CAA48786] vs. nGNL (NCBI accession no. ZP_00110023). (*B*) rSMP30 vs. zGNL (NCBI accession no. CAA47637). Two regions homologous among rat SMP30, nGNL, and zGNL are boxed in *A* and *B*.

SMP30 cDNA in *E. coli*. Recombinant SMP30 protein was expressed as a maltose-binding protein (MBP) fusion protein by using a chaperone coexpression system, and a soluble cell lysate was prepared. In this lysate, cells expressing the MBP–SMP30 fusion had clear-cut GNL activity (546 ± 18 nmol/min per mg of protein, mean ± SEM, $n = 3$) with D-glucono-δ-lactone used as a substrate, whereas the lysate of control cells (expressing a fusion of MBP with the α-fragment of β-gal) had no such activity. We further ascertained that the SMP30 fusion was the entity possessing GNL activity by subjecting this lysate containing the MBP–SMP30 fusion to native gel electrophoresis in triplicate and electroblotting onto a polyvinylidene fluoride membrane. The three parts of the membrane were respectively stained for GNL activity or immunochemically with anti-MBP or anti-SMP30 antibody. The bands stained in these three ways appeared at the same position (Fig. 2, lanes marked "2"). In contrast, a lysate of the cells expressing a fusion protein of MBP with the α-fragment of β-gal as a control did not contain any protein that was stained positive for GNL activity (Fig. 2 *A* and *C*, lane 1).

Enzymatic Characterization of SMP30. Subsequently, we measured GNL activity with a reaction mixture containing 10 mM D-glucono-δ-lactone, 75 μM $ZnCl_2$, and 0.42 μg/ml purified rat SMP30. The SMP30 hydrolyzed D-glucono-δ-lactone with a specific activity of 226 μmol/min per mg at an optimal pH of 6.4 with a linear increase up to an enzyme concentration of 0.42 μg of protein per ml (Fig. 8 *A* and *C*, which is published as supporting information on the PNAS web site). However, GNL activity was below the limit of detection in the absence of Zn^{2+}. Because a maximum level of GNL activity was observed at a Zn^{2+} concentration of 75 μM (Fig. 8*B*), this amount of Zn^{2+} was used in all experiments for enzymatic characterization.

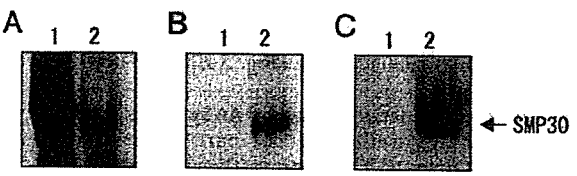

Fig. 2. Immunoblot analysis after native PAGE and activity staining of recombinant rat SMP30. Samples were electrophoresed on a native polyacrylamide gel, and the proteins on the gel were electroblotted onto a membrane. Detection of specific proteins was carried out with anti-MBP antibody (*A*), anti-rat SMP30 antibody (*B*), and activity staining (*C*). To stain for enzyme activity, D-galactono-γ-lactone was used as substrate. Lane 1, the lysate of *E. coli* cells expressing a fusion of MBP with β-gal α-fragment (control); lane 2, the lysate of *E. coli* cells expressing a fusion of MBP with rat SMP30. The arrow shows the position of a fusion of MBP with rat SMP30.

Other divalent metal ions were also tested at a concentration of 75 μM in the standard assay mixture. Only Mn^{2+} ions were effective, giving 27% of the enzyme activity observed with Zn^{2+} (Fig. 8*B*), whereas Mg^{2+}, Co^{2+}, Ca^{2+}, and Cd^{2+} ions gave no activity. However, slight enzyme activity (≪10%) was observed with 3 mM concentrations of these metal ions and a 10-fold higher concentration of SMP30 (4.2 μg/ml) (data not shown).

Next, we studied the kinetics of the GNL reaction. Hyperbolic kinetics were normal (Fig. 9, which is published as supporting information on the PNAS web site), and a Lineweaver–Burk plot of the data yielded an apparent K_m value of 9.4 mM and a V_{max} value of 345 μmol/min per mg (Fig. 9 *Inset*). The lactonase activities for a variety of sugar lactones by SMP30 are summarized in Table 2, which is published as supporting information on the PNAS web site. D-glucono-δ-lactone was the best substrate. SMP30 also hydrolyzed L-glucono-δ-lactone, D-gulono-γ-lactone, L-gulono-γ-lactone, D-galactono-γ-lactone, and L-galactono-γ-lactone, indicating that SMP30 has broad substrate specificity for aldonolactones. D-aldonolactones were better substrates than the corresponding enantiomers. SMP30 had no detectable hydrolyzing activity toward D-ribono-γ-lactone, D-mannono-γ-lactone, or D-glucoheptono-γ-lactone.

An Essential Role of SMP30 in AA Biosynthesis. To examine whether these substrates are attacked only by SMP30 in the rat liver, we compared lactonase activity in livers from SMP30Y$^-$ and SMP30Y$^-$ mice. Liver extracts from SMP30Y$^+$ mice hydrolyzed D-glucono-δ-lactone, D-gulono-γ-lactone, and D-galactono-γ-lactone, whereas those from SMP30Y$^-$ mice had no detectable

Table 1. Absence of GNL activity in livers from SMP30 knockout mice

Substrate	Specific activity, μmol/min per mg	
	SMP30Y+	SMP30Y−
D-glucono-δ-lactone	9.0 ± 0.6	ND
D-gulono-γ-lactone	0.5 ± 0.1	ND
D-galactono-γ-lactone	0.4 ± 0.1	ND

The hydrolytic activities for the substrates of SMP30 were determined by the method described in *Materials and Methods*. The values are the average ± SEM for livers from five animals. ND, no detectable enzyme activity.

hydrolyzing activity toward these lactones (Table 1). Clearly, therefore, SMP30 is a unique enzyme that effectively hydrolyzes various aldonolactones in the liver. Because the lactonization of L-gulonic acid to L-gulono-γ-lactone, the reverse reaction of the lactonase reaction, is the penultimate step of AA synthesis, we investigated the role of SMP30 in this metabolic process by using SMP30 knockout mice. Ten days after weaning at the age of 30 days, SMP30Y− and SMP30Y+ mice, six each, were fed a vitamin C-deficient diet. One of the knockout mice started to lose weight after 25 days of consuming this diet (at an age of 65 days), walked with an abnormal gait after 31 days, and died after 37 days. The average body weight of the other five knockout mice started to decrease after 56 days of the vitamin C-deficient diet (at an age of 96 days) (Fig. 3*A*); their gait became abnormal at that time, and they died by the 106th to 135th days of this dietary deficiency. The AA level in plasma of SMP30Y− mice after 106 days of consuming the deficient diet was <1% of that in SMP30Y+ mice (Fig. 3*B*). The livers and kidneys of SMP30Y− mice at the time of death contained <1.6% of the AA levels in the SMP30Y+ mice (Fig. 3 *C* and *D*).

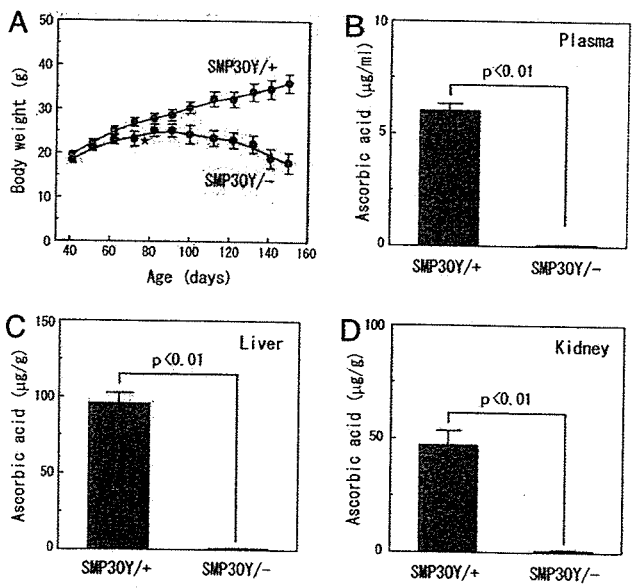

Fig. 3. Body weight changes and AA levels in the plasma, livers, and kidneys of SMP30Y− and SMP30Y+ mice. SMP30Y− and SMP30Y+ mice, six each, were weaned at 30 days of age and fed autoclaved mouse chow (containing ≈55 mg of AA per kg) for 10 days; then, they were fed a vitamin C-deficient diet until all SMP30Y− animals were dead. (*A*) Body weight changes of SMP30Y− (pink circles) and SMP30Y+ (green circles) mice. One SMP30Y− mouse died after 37 days (indicated by star), and the others died after 106–135 days of consuming the vitamin C-deficient diet. (*B–D*) Blood was taken from all tested animals (six WT and five knockout mice) after 106 days of this diet, and AA levels in the plasma (*B*) were measured. All mice were killed after 136 days of receiving the deficient diet, and AA levels in the liver (*C*) and kidney (*D*) were measured. Except for blood, all specimens of SMP30Y− mice were taken after death. Values are expressed as mean ± SEM of five or six animals.

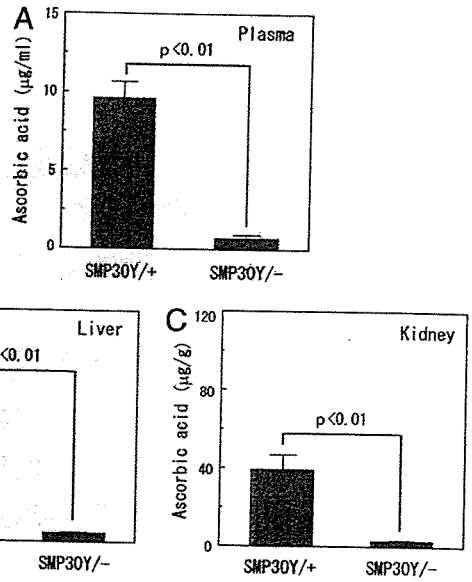

Fig. 4. AA levels in the plasma, livers, and kidneys from SMP30Y− and SMP30Y+ mice that were fed autoclaved mouse chow. SMP30Y− and SMP30Y+ mice, four each, were weaned at 30 days of age and fed autoclaved mouse chow (containing ≈55 mg of AA per kg) for 80 days (age 110 days). AA levels were then measured in their plasma (*A*), livers (*B*), and kidneys (*C*). Values are expressed as mean ± SEM of four animals.

For the previous studies, our SMP30Y− mice were fed autoclaved mouse chow after weaning, and this food contains ≈55 mg/kg of vitamin C. When we assessed the vitamin C status of such mice after 80 days of eating autoclaved chows, their plasma, livers, and kidneys contained only 6–8% of the AA values in the WT mice (Fig. 4). Thus, the knockout mice that were fed autoclaved mouse chow proved to be severely vitamin C-deficient.

Osteogenic Disorder of SMP30 Knockout Mice. Because thin, brittle bones with a tendency to fracture are known as characteristic manifestations of scurvy, we checked the skeletal structure of SMP30Y− and SMP30Y+ mice by x-ray examination after they had consumed the vitamin C-deficient diet for 59 days (at an age of 99 days) (Fig. 5 *A* and *B*). Fracture at the distal end of their femurs (Fig. 5*B Inset*) and rachitic rosaries at the junction of costae and costal cartilages (Fig. 5*B*) were prominent in a SMP30Y− mouse (Fig. 5*D*), but not a SMP30Y+ mouse (Fig. 5*C*). Moreover, subcranial total bone mineral density (BMD) and body fat were significantly decreased in SMP30Y− mice compared with SMP30Y+ mice (Fig. 5 *E* and *F*).

Occurrence of an Alternative Pathway of AA Synthesis. Two pathways were proposed as forming the last part of the AA synthetic pathway (12). Obviously, the main pathway of this process dealt with here includes the steps from D-glucose to L-gulonic acid (detailed on the left side of Fig. 6*A*). However, for the formation of L-gulono-γ-lactone, the immediate precursor to AA, another pathway branches from D-glucuronic acid (Fig. 6*A*, right side). To clarify whether the latter pathway exists in the mammalian metabolism, we injected D-glucurono-γ-lactone i.p. into SMP30Y− mice and measured the amount of AA excreted in their urine. We used the lactone for delivery of D-glucuronic acid

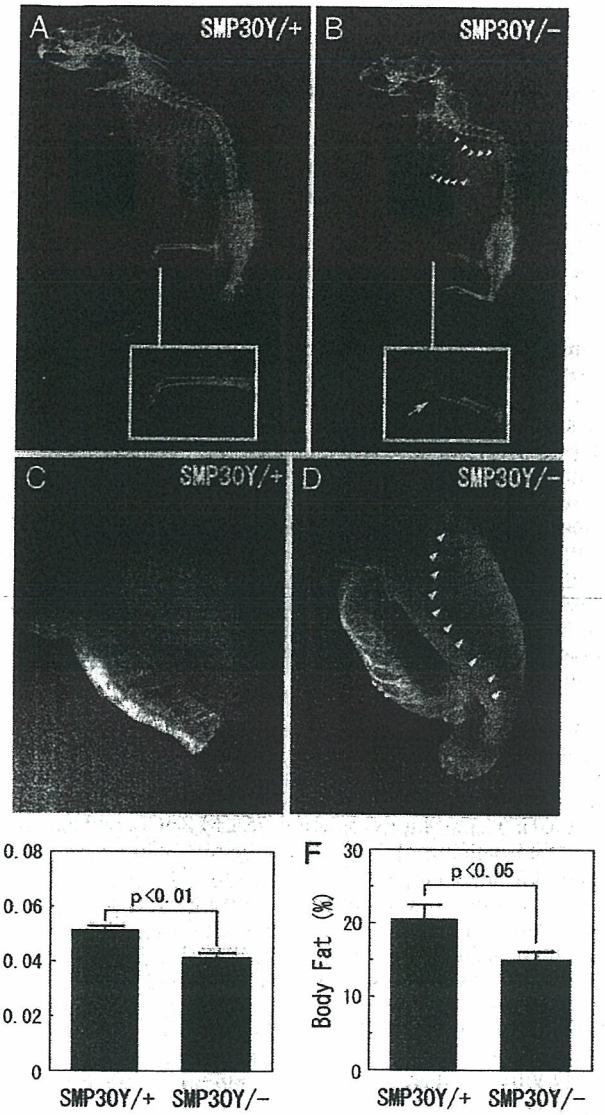

Fig. 5. Osteogenic disorder of SMP30 knockout mice. SMP30Y$^-$ and SMP30Y$^+$ mice at an age of 40 days were fed a vitamin C-deficient diet for 59 days (animals' age was 99 days). (*A–D*) X-ray images show the skeletal structures of SMP30Y$^+$ (*A*) and SMP30Y$^-$ (*B*) mice. *Insets* show enlargements of the femoral region; an arrow points to the distal femur fracture of a SMP30 knockout mouse. A rachitic rosary of the SMP30Y$^-$ mouse observed after evisceration (*D*) is compared with that area in a control mouse (*C*). Arrowheads in *B* and *D* indicate a rachitic rosary at the junction of costae and costal cartilage. (*E* and *F*) Subcranial total BMD (*E*) and body fat percentage (*F*) of SMP30Y$^-$ and SMP30Y$^+$ mice were determined by PIXImus2 densitometry as described in *Materials and Methods*. Values are expressed as mean ± SEM of five or six animals.

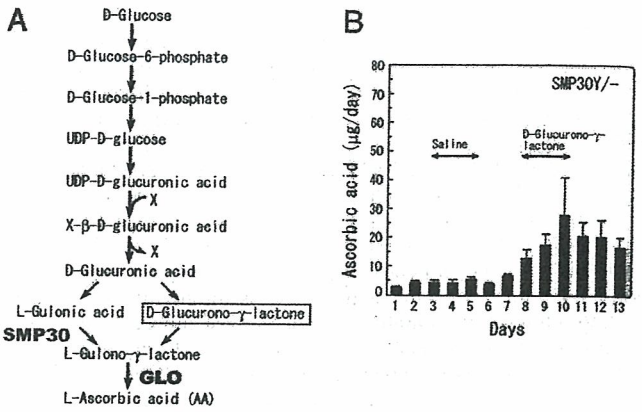

Fig. 6. Increased excretion of AA in the urine after administration of D-glucurono-γ-lactone. (*A*) The pathway of AA biosynthesis. The pathway from D-glucose to L-gulonic acid is shared with that of early steps in the uronic acid cycle. X is a conjugating molecule for glucuronidation. GLO, L-gulono-γ-lactone oxidase. (*B*) SMP30Y$^-$ mice were fed autoclaved mouse chow for 60 days after weaning and were housed individually in metabolic cages starting on day 1. Saline was injected i.p. from day 3 to day 5; then, D-glucurono-γ-lactone (0.7 mg/g of body weight) dissolved in saline was injected i.p. from day 8 to day 10. Urine samples were collected, and their AA concentrations were measured. Values are expressed as mean ± SEM of four SMP30Y$^-$ mice.

into liver cells, where AA synthesis occurs, because the lactone would be more easily incorporated into the cells than D-glucuronic acid and would come into equilibrium with this acid by catalysis of uronolactonase (12, 13). As a result, the excretion of AA was appreciably increased by the injection, albeit in a small amount, whereas AA excretion was not affected by the saline injected as a control (Fig. 6*B*). Thus, the alternative pathway was clearly operational here, regardless of its small flux.

Discussion

This study provides unequivocal evidence that SMP30 is the bona fide GNL in the AA biosynthetic pathway of mammals. In support, (*i*) SMP30 purified from the rat liver exhibited GNL activity (Fig. 7 and Table 2), (*ii*) a partial amino acid sequence of GNL purified from rat liver was identical to that of the reported sequence of rat SMP30, and (*iii*) the GNL was recognized by antibody directed to rat SMP30. Moreover, recombinant rat SMP30 expressed in *E. coli* showed GNL activity (Fig. 2). Overall, the purified SMP30 had the same substrate specificity toward multiple lactones as previously reported for GNL (7, 11, 13, 14). With respect to the requirement for metal in this process, Zn^{2+} and Mn^{2+} were both effective activators, although it was previously reported that Mn^{2+} was dominantly effective but that Zn^{2+} had no effect. This discrepancy is possibly due to differing experimental settings (11, 13, 14).

Measurements of GNL activity disclosed that the liver extract of SMP30 knockout mice lacked any such activity under conditions in which the WT extract was markedly active for three known substrates of GNL (Table 1). This outcome indicates that SMP30 is the unique lactone-hydrolyzing enzyme for these substrates in the liver. An essential role of SMP30 in AA biosynthesis in mice was evidenced by a nutritional study using SMP30 knockout mice. AA is produced from the ultimate hexose precursor D-glucose, and, in this pathway, L-gulonic acid, an intermediary metabolite of the uronic acid cycle, is lactonized to form L-gulono-γ-lactone, which in turn is oxidized to AA (Fig. 6*A*). GNL is known to catalyze the former reaction (8–10). In our experiments, scurvy developed in SMP30 knockout mice that were fed a vitamin C-deficient diet (Figs. 3 and 4). Their symptoms of scurvy included bone fractures, rachitic rosaries, and premature death by 135 days after institution of the vitamin C-deficient diet. In view of this fact, one can understand the phenotypes of SMP30 knockout mice mentioned in the Introduction (abnormally low body weight, shortened life span, susceptibility to hepatic apoptosis, etc., compared with WT mice). For our previous studies (2–4), these mice were fed autoclaved mouse chow, which we now know contains too little vitamin C to maintain normal levels of AA in tissues (Fig. 4). Accumulations of triglycerides, phospholipids, and cholesterol in the livers of these knockout mice may be associated with impaired fatty acid oxidation, probably because of decreased synthesis of carnitine, which plays a role in the transport of

long-chain fatty acids into mitochondria. AA is required as a cofactor in two hydroxylation reactions in carnitine biosynthesis (15). In fact, AA-deficient guinea pigs were shown to have abnormalities of lipid metabolism, such as hyperlipidemia and hypercholesterolemia (16). Another clinical feature of young SMP30 knockout mice is enlargement of alveolar airspaces compared with those of WT mice (2). A similar change was reported in ODS (osteogenic disorder Shionogi) rats that survived for a long time on a vitamin C-deficient diet (17). However, never before did we observe scurvy symptoms in the knockout mice that were fed autoclaved mouse chow, despite their smaller body size and shorter life span (3, 4). Assuming that an average weight of mice is 25 g and that the amount of chow taken per day is 4 g (18), SMP30 knockout mice ingest <0.01 mg/g of body weight per day. Based on the observation that 0.02 mg/g of body weight per day cannot sustain normal body function in a scurvy-prone mouse whose L-gulono-γ-lactone oxidase gene was deleted (19), the SMP30 knockout mice seem not to have ingested enough vitamin C. Probably, a small amount of AA may be synthesized through the alternative pathway (Fig. 6*A*) previously proposed based on an enzymatic study (20) and demonstrated here in SMP30 knockout mice. Furthermore, the absence of GNL may lead to decreased degradation of AA, because GNL can hydrolyze the lactone ring of dehydroascorbic acid, the oxidation product of AA, to 2,3-dioxo-L-gulonic acid, as formerly reported (20).

Because SMP30 is abundant in the kidney and also present, although in lesser amounts, in other organs (21), this protein must have some function other than AA synthesis, which does not occur at all these sites. SMP30 may prevent the production of glycated proteins by hydrolyzing D-glucono-δ-lactone. It is possible that this lactone is formed from D-glucose by glucose dehydrogenase *in vivo*, and it may be involved in glycation of proteins. In fact, human and rat hemoglobin was shown to be glycated with D-glucono-δ-lactone (22). Glycated proteins, especially advanced glycation end products, are known to cause the deterioration of cellular functions; therefore, SMP30 may protect cells from such an effect.

Materials and Methods

Chemicals. L-glucono-δ-lactone, D-gulono-γ-lactone, L-gulono-γ-lactone, L-galactono-γ-lactone, D-ribono-γ-lactone, D-glucoheptono-γ-lactone, and D-mannono-γ-lactone were purchased from Sigma-Aldrich. D-glucono-δ-lactone, D-galactono-γ-lactone, and other reagents were purchased from Wako Pure Chemical (Osaka).

Animals. Male Wister rats, 3–9 months of age, were obtained from the Animal Facility at Tokyo Metropolitan Institute of Gerontology, and their livers were used as a source of purified SMP30. For purification of GNL, 10-week-old male Wister rats purchased from Kiwa Laboratory Animals (Misato-cho, Japan) were used. SMP30 knockout mice were previously generated with the gene-targeting technique (3), and heterozygous female mice ($SMP30^{+/-}$) were mated with male knockout mice ($SMP30Y^{-}$) to produce knockout and WT ($SMP30Y^{+}$) littermates. These littermates were fed autoclaved mouse chow (CRF-1; Charles River Breeding Laboratories) ad libitum with free access to water and used for measurement of GNL activity in the liver when the animals were 6 months old. The autoclaved chow contained ≈55 mg of AA per kg as determined at the time of experimentation.

In a nutritional study, $SMP30Y^{-}$ and $SMP30Y^{+}$ mice were weaned at 30 days of age and fed autoclaved mouse chow for 10 days, followed by a vitamin C-deficient diet (CL-2; CLEA Japan, Tokyo). Throughout the experiments, animals were maintained on 12-h light/dark cycles in a controlled environment. All experimental procedures using laboratory animals were approved by the Animal Care and Use Committee of Tokyo Metropolitan Institute of Gerontology.

Purification of SMP30 from Rat Liver. SMP30 was purified from a soluble fraction of rat livers as described in ref. 5. Briefly, liver homogenate was fractionated by ammonium sulfate precipitation followed by a successive series of chromatographies on DEAE-Sephacel, Phenyl Sepharose CL-4B, and Sephacryl S-200 HR columns (all from Amersham Pharmacia Biosciences). The elution of SMP30 was followed by the dot-blot immunoassay described in ref. 5. The purified SMP30 was stored at −70°C until use.

Purification of GNL and Sequence Analysis of Its Peptide. GNL was purified from rat livers according to the method of Grossman and Axelrod (11), with slight modifications. Briefly, a soluble fraction of the liver homogenate was heated at 50°C for 30 min, and the resulting soluble fraction was fractionated with ammonium sulfate. The fraction with GNL activity was further purified by successive chromatographies on columns of Sephadex G-150 (Amersham Pharmacia Fine Chemicals), Resource Q (Amersham Pharmacia Biosciences), and Bio-Gel HTP (Bio-Rad). After the final preparation was subjected to SDS/PAGE, the main band was excised, and the protein in the gel was digested with trypsin. One of the peptides produced was sequenced through the custom service of APRO Life Science Institute (Naruto, Japan).

GNL and Related Activities. GNL activity was measured by the change in absorbance of the pH indicator *p*-nitrophenol caused by free acid formation from the lactone (23). The standard mixture contained 10 mM D-glucono-δ-lactone, 10 mM Pipes (pH 6.4), 0.25 mM *p*-nitrophenol, 75 μM $ZnCl_2$, and an enzyme in a total volume of 1 ml. The substrate solution was freshly prepared immediately before the assay. The reaction was followed by monitoring a decrease in absorbance at 405 nm, and the acid production rate was determined with a calibration curve obtained by using known amounts of HCl. The rate of spontaneous hydrolysis of the lactone was subtracted from the total rate. To assess whether a divalent metal ion was required for GNL activity, we tested $ZnCl_2$, $MnCl_2$, $MgCl_2$, $CoCl_2$, $CaCl_2$, and $CdCl_2$ in this regard and then determined the hydrolyzing activity for other lactones with the same procedure, except for the substrate.

Lactonase activity was then analyzed in livers removed from mice and homogenized with ice-cold homogenization buffer (10 mM Tris·HCl, pH 8.0/1 mM phenyl methanesulfonyl fluoride) for 30 s at high speed with a Polytron homogenizer. The homogenate was centrifuged at 10,000 × *g* for 10 min. The protein concentration of the sample was determined by BCA protein assay (Pierce) using BSA as a standard. The lactone-hydrolyzing activity was assayed by using various lactones under the standard conditions described above. In the purification of rat GNL, lactonase activity was measured by recording pH change with a pH meter, essentially as described in ref. 24.

Expression of Recombinant Rat SMP30. Total RNA was prepared from a rat liver and used to produce a single-strand cDNA with SuperScript II RNase H^{-} reverse transcriptase (Life Technologies, Rockville, MD) following the manufacturer's protocol. A SMP30 cDNA was amplified by PCR from this cDNA such that an EcoRI site would be produced at the both ends of the product. The PCR was carried out by using *PfuUltra* DNA polymerase (Stratagene) with a sense primer (5′-GAATTCATGTCTTCCATCAAGATTG-3′) and an antisense primer (5′-GAATTCTTACCCTGCATAGGAATATG-3′). The amplified DNA was digested with EcoRI and inserted into the EcoRI site of the *E. coli* expression vector pMAL-c2x (New England Biolabs). The